The Pennsylvania State University

The Graduate School

The College of Earth and Mineral Sciences

DEEP PORE PRESSURES AND SEAFLOOR VENTING IN THE AUGER BASIN, GULF OF MEXICO.

A Thesis in

Geoscience

by

Matthew Reilly

Submitted in Partial Fulfillment
of the Requirements
for the Degree of

Master of Science

December 2008

The thesis of Matthew Reilly was reviewed and approved* by the following:

Peter B. Flemings
Adjunct Professor of Geosciences
Thesis Advisor

Demian Saffer
Associate Professor of Geosciences

Turgay Ertekin
Professor of Petroleum and Natural Gas Engineering
George E. Trimble Chair in Earth and Mineral Sciences

Katherine H. Freeman
Professor of Geosciences
Associate Head for Graduate Programs and Research

*Signatures are on file in the Graduate School

ABSTRACT

This thesis is composed of three Chapters.

Chapter 1 is a preface that outlines the degree program and components of my thesis. Chapter 2 is the main body of the thesis; it is an investigation into pore pressures in the Auger basin and how they are related to fluid venting at the seafloor. I map the distribution of subsurface pressures in thick interconnected sand bodies that are present across the Auger Basin, Gulf of Mexico. I show that overpressures are nearly constant across as many as 12 miles (19km) in the basin. Using 3D seismic and pressure data I show that the extrapolation of pressures along the hydrostat results in accurate prediction of reservoir pressures over basin-scale distances. Furthermore, at the sand crest, pressures are high enough to hydraulically fracture the overlying shales and therefore dynamically constrain the sand pressures by way of a leak point overlain by mud volcanoes. The expelled material from multiple mud volcanoes in the Auger Basin covers an area over 25km² and may be a useful analogy for present day natural disasters.

Chapter 3 is an insert in the back pocket of this thesis. Chapter 3 is a characterization of the N and O sands of the Auger basin, Gulf of Mexico. It is the result of the collaboration of the four members of the Petroleum Geosystems Initiative.

TABLE OF CONTENTS

LIST OF FIGURES v

LIST OF TABLES vii

ACKNOWLEDGEMENTS viii

Chapter 1 Preface 1

Chapter 2 Deep Pore Pressures and Seafloor Venting in the Auger Basin, Gulf of Mexico 3

- Introduction 3
- Regional Setting and Stratigraphy of the Auger Basin 5
- Structure and Stratigraphic Architechture 11
- Pressure and Stresses 16
- Reservoir Pressures 19
- The Seafloor Vent Complex 29
- Discussion 34
- Conclusions 38
- Tables 40
- Appendix A: Depth Conversion Velocity Model 46
- Appendix B: Estimation of Overburden Stress 48
- Appendix C: Calculation of Fluid Flux through a Sandbody 50
- References 53

LIST OF FIGURES

Figure **1-a**: Amplitude extraction of the Auger Basin with structural overlay 7

Figure **1-b**: Overburden/pore pressure map of the Q sand with structural overlay 7

Figure **2a**: Seismic cross section of the Auger Basin with illustrations.....8

Figure **2b**: Seismic cross section of the sand crests 8

Figure **3**: Structure maps of the S, R, Q and P sands 10

Figure **4-a**: Type logs of the P sand with pressure data 14

Figure **4-b**: Type logs of the Q sand with pressure data 14

Figure **4-c**: Type logs of the R sand with pressure data.....15

Figure **4-d**: Type logs of the S sand with pressure data.....15

Figure **5a**: Principle stresses of the minibasin 17

Figure **5b**: Reservoir pressures of the Auger Basin 18

Figure **6-a**: Field scale structure map of the Q sand with hydrocarbon area delineated 22

Figure **6-b**:Field Scale pressure -depth plot for the Q sand 22

Figure **7-a**: Reservoir presures of the P sand 26

Figure **7-b**: Reservoir presures of the Q sand 26

Figure **7-c**: Reservoir presures of the R sand 27

Figure **7-d**: Reservoir presures of the S sand 27

Figure **8-a**: Basin scale pressure-depth plot of the Q sand 28

Figure **8-b**: Fluid pressure gradient plot of the Q sand.....28

Figure **9**: 3D map of the seafloor expulsion features 31

Figure **10-a**: Flattened seismic timelslice 16ms below the seafloor 33

Figure **10-b**: Flattened seismic timelslice 52ms below the seafloor.....33

Figure **10-c**: Shallow time cross section of expulsion feature 4 33

Figure **11**: Appendix A, Depth Conversion Velocity Model 47

Figure **12**: Appendix B, Estimation of Overburden 49

LIST OF TABLES

Table **1**: Comparison of velocity data. 41

Table **2**: Principle stresses in relation to sand structur 42

Table **3**: LOT data summary. 43

Table **4**: Nomenclature table. 44

ACKNOWLEDGEMENTS

I would like to thank my advisor Peter Flemings. I would like to thank D. Saffer, T. Ertekin, R. Slingerland, C. Bohn, R. Skarbek, D. Sawyer, J. Schneider for useful discussions and also Heather Nelson for invaluable technical support. I would like to thank my Geosystems teammates for their work and friendship. I would like to thank Shell Oil and CGGVeritas for access to seismic data across the Auger Basin. I would also like to thank Tom Wilson, Sue Waters and Cristina Arroyo at Shell Oil for providing well log data and pressure measurements. Landmark Graphics Seisworks® 3D, Paradigm Geolog® and the freeware Generic Mapping Tool program were the primary software tools used in this study. This research was supported by the Penn State GeoSystems Initiative (Shell and Chevron), Newfield Exploration, the GeoFluids III Consortium and the Heller Foundation.

Chapter 1

Preface

This thesis is composed of a preface (Chapter 1), a main body (Chapter 2), appendices, and an insert (Chapter 3) in the back pocket. The preface explains the content and order of the constituents of the thesis and distinguishes between the team and my individual contributions.

The main body of the thesis (Chapter 2) presents my individual investigation the pore pressures of deep reservoir sands in the Auger Basin and their relation to surface expulsion features.

The insert in the back pocket (Chapter 3) is a reprint of the paper, 'Accommodation history, reservoir architecture, and production behavior in the N and O sands of the Auger Field, deepwater Gulf of Mexico.' This paper is the result of the collaboration of the four members of the Petroleum Geosystems Initiative Team 4. The Petroleum Geosystems Initiative is a multi-disciplinary M.S. program. This program consists of four graduate students: Charles Bohn III, Matthew Reilly, Doruk Seren, and Joseph Valenti. Each approached the analysis of Auger Field in the Gulf of Mexico from the disciplines of geology, geophysics, petrophysics, and petroleum engineering. This work was presented in poster format by Bohn at the American Association of Petroleum Geologists (AAPG) Annual Convention in 2008 (Bohn *et al.*, 2008). Since the content of this paper contains background information relevant to this thesis and since the paper has four co-authors, the reprint is included in the back cover of this thesis.

The following is a reproduction of the email from Regina Vasilatos-Younken (Senior Associate Dean of the Graduate School) to Peter B. Flemings (thesis advisor) regarding the inclusion of this co-authored paper:

From: Regina Vasilatos-Younken <rxv@psu.edu>

To: flemings@geosc.psu.edu

cc: pml3@psu.edu

Subject: Re: Email From Flemings in Preparation for 11:15 tel. call today.

Peter - As we discussed today, a mutually agreeable solution to your request is to have the students who are participating in the GeoSystems Initiative position their individual research chapters in the body of the thesis (e.g., following an appropriate literature review and introduction), which would then be followed by an introduction to the collaborative project and paper product, and referring the reader to the paper (to be formatted as a journal article/preprint) contained in a pocket on the back cover of the hard bound thesis. This paper would list all four students as co-authors. When the students submit their respective theses to the thesis office, they need to submit the appropriate number of copies of this paper for each copy of the thesis to be bound, and indicate that it is to go in a pocket on the back cover. There is no extra charge by the University Libraries to the individual student for these special accommodations in the binding process for the "official copy" that will be archived in the Library.
If you have any questions regarding this approach, please don't hesitate to contact me. Congratulations on what sounds like an excellent experience for the students and one which prepares them in a meaningful way for working collaboratively in the "real world" of research.

Jean

Regina Vasilatos-Younken, Ph.D.

Professor of Endocrine Physiology & Nutrition, and
Senior Associate Dean of the Graduate School
114 Kern Graduate Building
The Pennsylvania State University
University Park, PA 16802
Tele: (814) 865-2516
Fax: (814) 863-4627
E-mail: rxv@psu.edu

Chapter 2

Deep Pore Pressures and Seafloor Venting in the Auger Basin, Gulf of Mexico

Introduction

Natural oil and gas seeps are widespread across the Gulf of Mexico slope, West Africa, and other prolific hydrocarbon regions worldwide (Graue, 2000; Hood *et al.*, 2002; Davies & Stewart, 2005). Such seeps or seafloor expulsion features have been associated with mud volcanoes, hydrocarbon accumulations, drilling hazards, and climate change (Gaarenstroom *et al.*, 1993; MacDonald *et al.*, 2002).

Mud volcanoes have recently gained international attention due to the 2006 eruption of the Lusi mud volcano, Java Indonesia, which as of August 2008, covered an area of 7km², displaced 30,000 people and continues to expand at rates of 5000-180,000 m³ per day (Davies *et al.*, 2007; Mazzini *et al.*, 2007; Davies *et al.*, 2008; Tingay *et al.*, 2008). The Lusi eruption was first thought to have been triggered by the Ygakarta earthquake, but others have suggested that it was caused by a blow-out in a nearby gas exploration well (Mazzini *et al.*, 2007; Davies *et al.*, 2008; Tingay *et al.*, 2008). I show how the processes behind subsurface fluid flow and seafloor venting in the Auger Basin, Gulf of Mexico, are similar to those artificially created in Java.

Seafloor expulsion features have been related to their deeper petroleum systems in order to understand trap integrity and reservoir pressures (Lupa *et al.*, 2002; Seldon & Flemings, 2005). Seeps have also been used to identify fluid migration pathways (Abrams *et al.*, 2000; Hood *et al.*, 2002) as well as to provide information about hydrocarbon source type and the organic maturity of the trapped hydrocarbons (Abrams, 2005; Abrams & Whelan, 2005).

Overpressure occurs when the rate of sedimentation is greater than the rate of fluid expulsion, causing the entrained fluids to support some of the overlying load (Harrison & Summa, 1991; Gaarenstroom *et al.*, 1993; Swarbrick *et al.*, 2000; Lupa *et al.*, 2002). Pressures in sandbodies with significant structural relief follow the hydrostatic gradient (Flemings *et al.*, 2002). These sands can be a conduits for large volumes of fluid flow (Flemings *et al.*, 2002). At the sand crest, pressures can be great enough to dilate fractures in the cap rock, causing fluid expulsion (Seldon & Flemings, 2005). In active plate margin settings, compressive forces are often cited as driving overpressured fluid and sediment expulsion (Birchwood, 1965; Higgins & Saunders, 1974; Khalilov & Kerimov, 1983; Yassir, 1987; Mazzini *et al.*, 2007). The presence of methane has led others to cite gas expansion/buoyancy as a driving mechanism for seal failure (Hedberg, 1974).

The seafloor expulsion features of the Auger Basin, Gulf of Mexico, have been the focus of numerous studies. They have been related to sea surface oil slicks (MacDonald *et al.*, 2000), gas hydrate accumulations (MacDonald *et al.*, 2002), mud venting (Kohl & Roberts, 1994), chemosynthetic communities (MacDonald *et al.*, 2000; Aharon, 2003) and radioactive barite deposits (Aharon, 2003). Paleo-vent complexes have also been discovered deep in the subsurface at Auger (Shew *et al.*, 1993).

I use direct pressure measurements from three producing oil fields within the Auger Basin to show sand pressure connectivity over large distances. I document that the water phase overpressures in four reservoir sands are approximately constant across as many as 19km (12 miles). This allows us to predict pressure throughout the basin. I show that beneath the Auger

mud volcanoes the crests of the reservoir sands have pore pressures that are equal to the least principle stress in the basin.

Regional Setting and Stratigraphy of the Auger Basin

The Auger Field lies 215 miles (345 km) southwest of New Orleans in 900m (3000 ft) of water depth (Figure 1a). Auger Basin is bounded by tabular salt bodies, which are topographically higher than the basin sediments (Figure 1a). It is the central basin in a series of three connected salt withdrawal mini-basins (Booth *et al.*, 2000). A salt ridge separates the Auger Basin from the Andros Basin to the east and the Tampa Basin to the south (Figure 1b). The salt dome in the center of the field was emplaced subsequent to the deposition of the Auger Basin reservoirs. This study interprets data from three producing fields in the Auger Basin: Auger, Cardamom and Macaroni (Figure 1).

There are seven main reservoirs in Auger Basin, all of which are Pliocene to Pleistocene aged turbidite deposits. They are termed the T, S, R, Q, P, O and N sands at Auger, Cardamom and Macaroni. The Q, R and P-sands are present at Auger and Macaroni and are produced at both locations. The S and T-sands also extend from Auger to Macaroni but are not produced at Macaroni (Figures 1, 2 and 3). The T, S, R, Q and P sands of the Auger Basin deepen and thicken to the south toward Macaroni Field and to the northeast into Andros Basin (Figure 1 and Figure 2), while the O and N sands cover a lesser aerial extent and were deposited as fan and channel systems.

Auger Field lies to the north, against the southern flank of the East Auger Salt Ridge, Cardamom is located on the northern flank of the East Auger Salt Ridge and Macaroni lies to the

south, on the flank of the southern basin bounding salt ridge (Figure 1 and Figure 3) (Booth *et al.*, 2003). The hydrocarbons in Auger and Cardamom Fields are trapped around the Auger salt dome (Figures 1, 2 and 3). Nineteen kilometers (12 miles) to the south, at Macaroni Field, the hydrocarbons are trapped against the southeastern flank of the surrounding salt. At Auger, the producing intervals are between 4.2km (14,000ft) and 6km (20,000ft) deep (Figures 1, 2 and 3). Macaroni Field is much deeper and has producing intervals from 6.4km (21,000ft) to 7.3km (24,000ft) (Figures 1, 2, and 3). The seismic reflections of the S, R, Q, P sands are uniform and easily mapped across the basin (Figure 2). The structural crests of the sands are all located on the eastern flank of the western margin of the basin, in blocks 380, 381,424, 468. At the seafloor, directly above the sand crests, are several mud volcanoes which line the edge of the basin (stars, Figures 1, 2 and 3).

Booth (2000) recognized two main styles of deposition at Auger Basin: ponded sheet sands, which are deposited when accommodation space exceeds the rate of sediment supply; and channelized sands, which are deposited when sediment supply overwhelms the available accommodation space. Ponded deposits produce aerially extensive sheet sands that offer excellent pressure communication (Booth *et al.*, 2000). During channelized deposition, the sand is confined to fans and channels and may also be amalgamated, eroded or shaled-out, resulting in poor pressure communication across large distances (Kendrick, 1999).

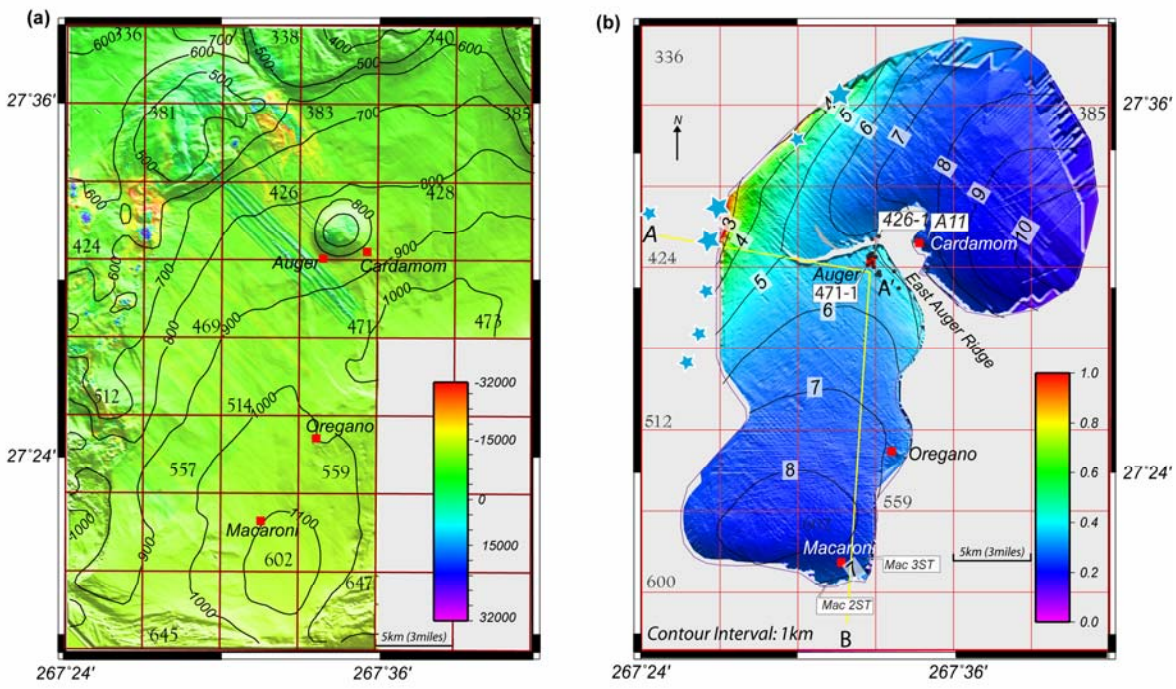

Figure **1-a**: Amplitude extraction of the seafloor with shaded structural relief and depth contours in meters. Positive amplitude flows (yellow-red) emanate from the mud volcanoes with negative amplitude tops (blues) on the western flank. Contour interval is 100m. **b:** Q-sand overpressure / Overburden ($P^* / \sigma_v h$) map with shaded structural relief and depth contours every 1km. Water phase pressure at the crest of the Q sand exceeds the maximum principle stress of the overlying mudstones. Vent locations are shown as stars. Location of cross section shown in Figure 2 is annotated A-A'-B.

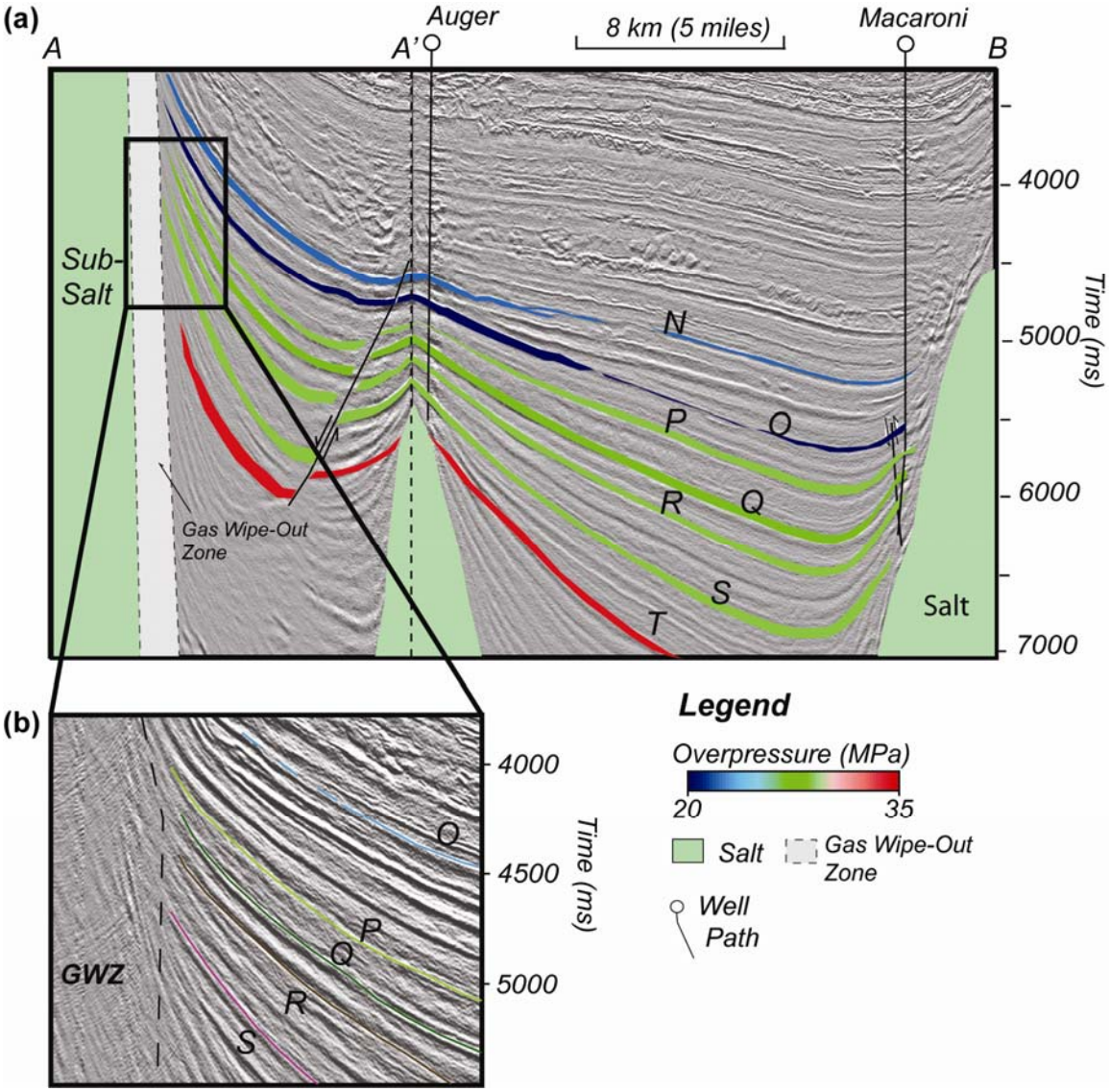

Figure **2a**: Cross section of the Auger Basin illustrates connectivity and geometry of sands across the basin from structural crest to base. Cross section A-A'-B is located in Figure 1b. Sands are colored in relation to their over pressure (P*). Notice the large amount of structural relief leading to the sand crest. **b:** Expanded view of the box in figure **a**. At the crests of the sands is the edge of Gas Wipeout Zone from the mud volcanoes above.

Sediments at Auger and Macaroni Field transition upwards from ponded sheet sand deposits to increasingly channelized deposits (McGee *et al.*, 1993; Booth *et al.*, 2000; Booth *et al.*, 2003). The T and S sands, are sheet sand deposits with excellent aerial continuity, whereas the O and N sands, are confined to channel and fan deposits. The R, Q and P have internal vertical transitions from basal sheet sands to increasingly channelized sands. The sheet sand deposits of the R, Q and P sands are thickest towards the center of the basin and thin outwards. Sediments also show a proximal to distal, or north-south, change in sand character (McGee *et al.*, 1993; Booth *et al.*, 2000; Booth *et al.*, 2003). In general sheet sand deposits are thicker and more common at Macaroni; at Auger there are more channelized deposits (McGee *et al.*, 1993; Booth *et al.*, 2000; Booth *et al.*, 2003).

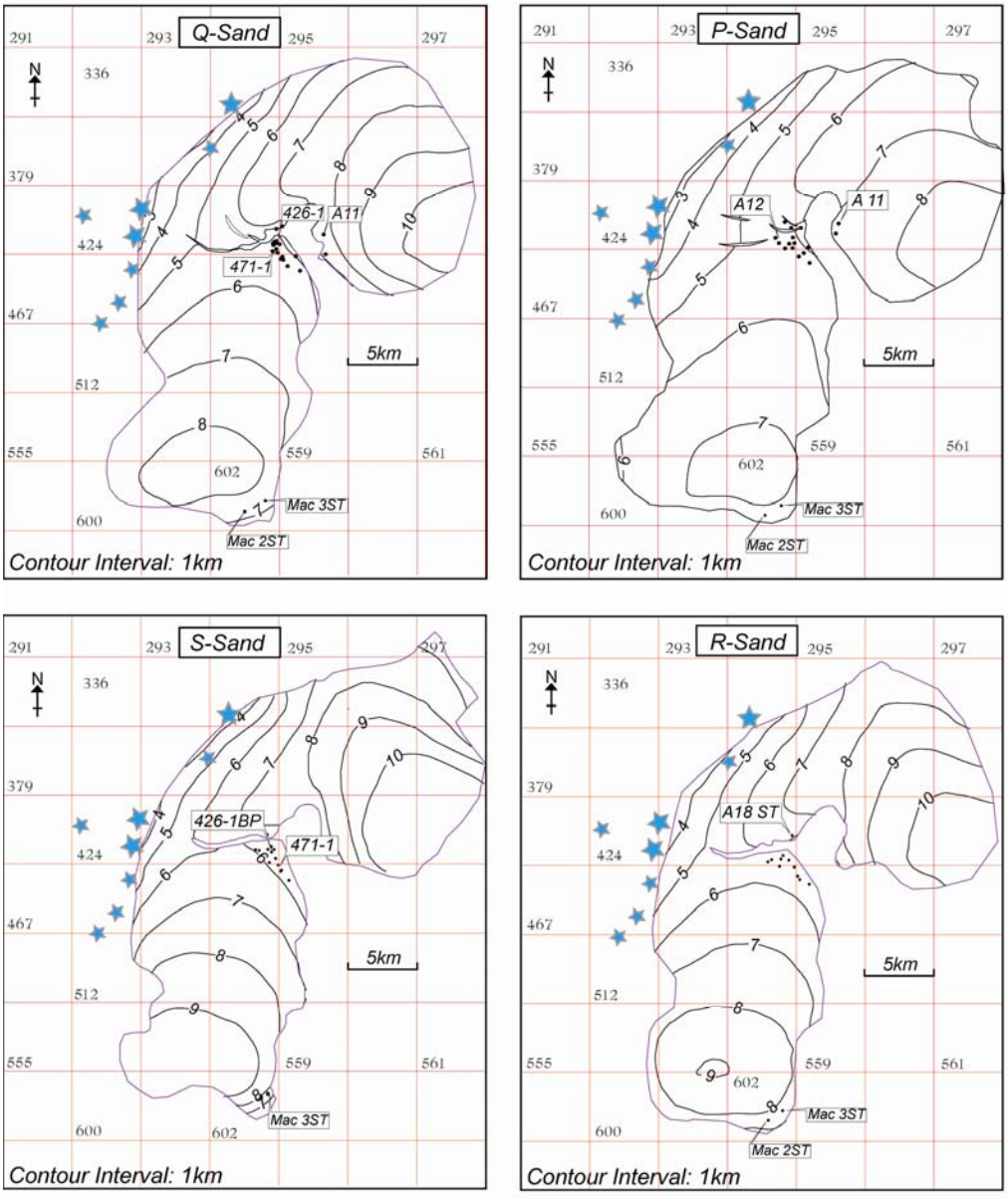

Figure **3**: Depth Structure maps of producing horizons at 1000m contours with OCS block overlay. Seafloor vent locations are shown with stars. Crest of Q and P sands is directly beneath GB424 whereas S and R sand crests are broader with highs in GB381. See Appendix A for depth conversion methodology

Structure and Stratigraphic Architecture

Stratigraphic architecture can determine the pressure connectivity of a sand body and its structural relief can influence the magnitude of overpressure (Kendrick, 1999; Flemings *et al.*, 2002). The S, R, Q and P sands have been the focus of numerous studies and consequently their stratigraphic architecture is well documented; all of these sand bodies are aerially extensive sheet sands (McGee *et al.*, 1993; Kendrick, 1999; Booth *et al.*, 2000). They have similar structural relief; their crests are to the northwest and they have two synclinal lows to the south and the northeast (Figure 3). Structure maps of the S, R, Q, P sands were constructed across the basin from 3D seismic and well data (Figure 3).

The accurate mapping of the seismic horizon is essential when comparing fluid pressures within a sandbody and the overburden pressures of the surrounding shales, as both are a function of depth. I use a zero-phase seismic survey and map on the maximum amplitude of the seismic trough. It is crucial to accurately map the highest point of the sand. Unfortunately this is challenging for the following reasons. There is a 'Gas Wipe Out Zone' (discussed later) at the sand crest, which may obscure the seismic horizons (Figure 2b). Secondly, the sands thin toward the crest and are hard to resolve (Figure 2b). I suggest that there may be significant error associated with these two problems and that the sand crests may extend higher than they have been mapped.

Maps were converted to depth using a dual layer velocity model (Appendix A). To account for the change in seafloor topography I calculated the depth to the seafloor using a water velocity of 15000m/s (4921ft/s). For each seismic horizon I used an average sediment velocity that was derived from well logs at Auger and Macaroni Field (veloctiy data for T, S, R, Q, P and

O sands can be found in Table 1). To account for velocity variation between Auger and Macaroni I linearly interpolated velocities with depth across the basin using Auger as my control point (Appendix A). The depth conversion error is estimated by taking the depth difference between the Auger velocity and interpolated velocity at the sand crest. For the example, the interpolated sediment velocity model for the Q sand results in a crest height that is 2390mbsf (meters below seafloor) (Table 1). Using the sediment velocity calculated at Auger results a Q sand crest height that is 3216mbsf (Table 1). The depth conversion error is 826m.

The S-sand seismic reflection is continuous across the basin and is thickest to the south in the centre of the basin (Figure 2 and Figure 3). The S sands continue to Macaroni where they have been penetrated by the Mac3ST well (Figure 4). The crest of the S sands is at 3422m (11227ft) True Vertical Depth Sub-Sea (TVDSS) and extends to 7620m (25000ft) TVDSS at its base (Figure 3). The R-sand can be traced on seismic across much of the basin. At Auger, Cardamom, and Macaroni the reservoir interval is composed of laterally extensive sheet sands. The crest of the R sands is at 3287m (10700ft) TVDSS and extends to 7315m (24000ft) TVDSS at its base (Figure 3).

The sheets sands of the Q sand series (Q2 and 3) are laterally extensive across the basin. The Q sand is present at Auger, Cardamom and Macaroni Fields (Figures 1, 2 and 3). Macaroni also contains an additional set of sands not found at Auger, (sequence 9,10 of (Booth *et al.*, 2003)) composed of thick erosive channels that incised progressively deeper to the south (Booth *et al.*, 2000; Booth *et al.*, 2003). The crest of the Q sands is at 2950m (9678ft) TVDSS and extends to 7010m (23500ft) TVDSS at its base (Figure 3 and Figure 5).

At Auger Field, the P sand consists of three thin and channel sands whereas at Macaroni, the P sand is a thick section of basal sheet sands grading into amalgamated sheet and channel sands. Compared to the S, R and Q sand intervals, the P-sand is more difficult to map on seismic data, as the thinner wet sands have little difference in acoustic impedance from the surrounding shales. At Auger Field this is especially noticeable as the P-sand is shadowed by the high amplitudes of the overlying N and O sands. The crest of the P sands is at 2860m (9383ft) TVDSS and extends to 7108m (23300ft) TVDSS at its base (Figure 3).

The T-sands consist of stacked sheet deposits similar to the overlying S-sand. The T sand seismic horizon thickens to the south towards centre of the basin but does not extend into Macaroni Field. The T-Sands have much less relief than the overlying S sands. The crest of the T sands is at 4220m (13845ft) TVDSS and extends to 10620m (34800ft) TVDSS at its base.

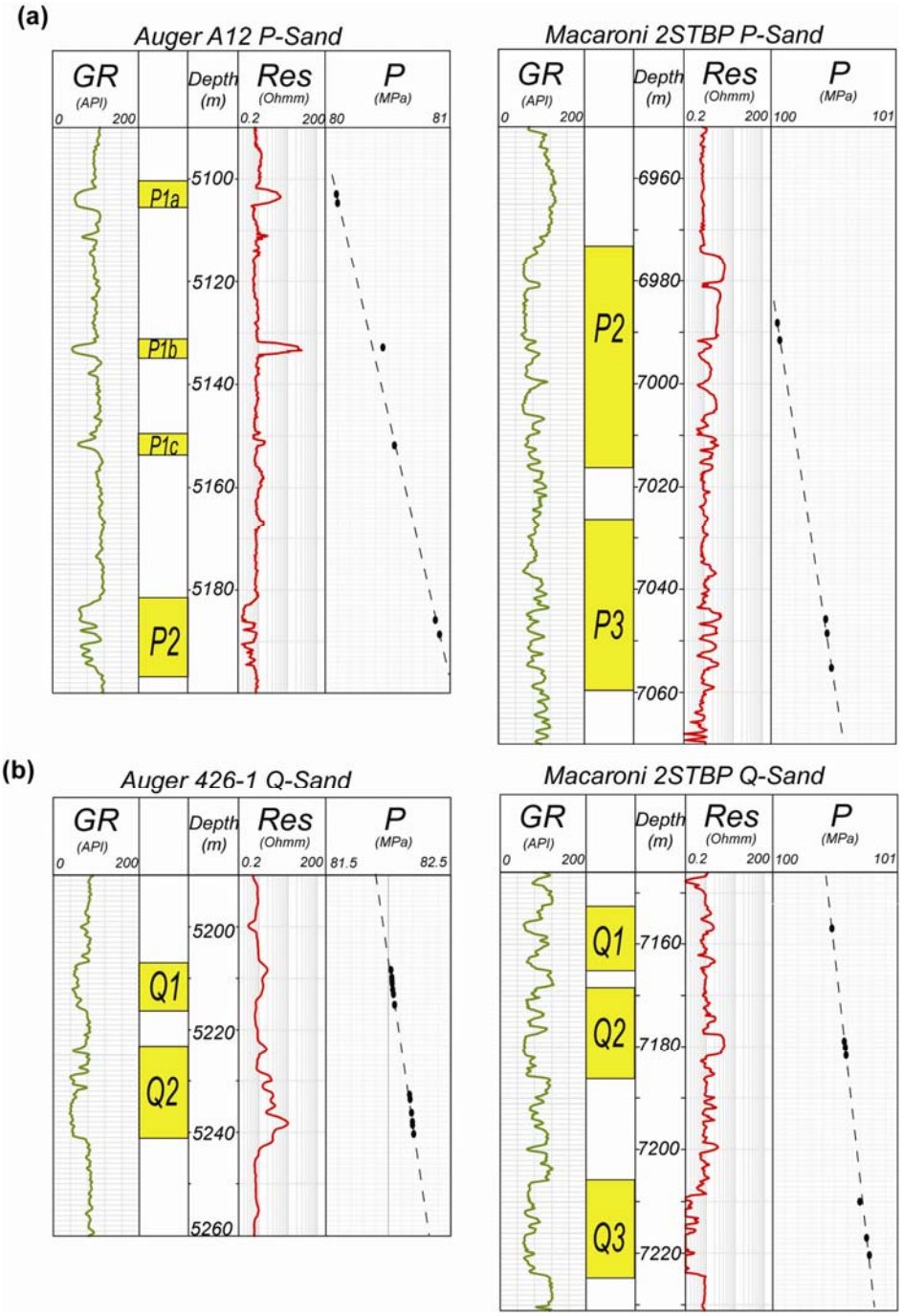

Figure **4-a**: Type logs of the P sand at Auger and Macaroni. **b:** Type log of the Q sand at Auger and Macaroni. There is an increase in sand thickness and net-to-gross from Auger to Macaroni in both sands. Oil-phase pressures follow the same gradient in respective sands.

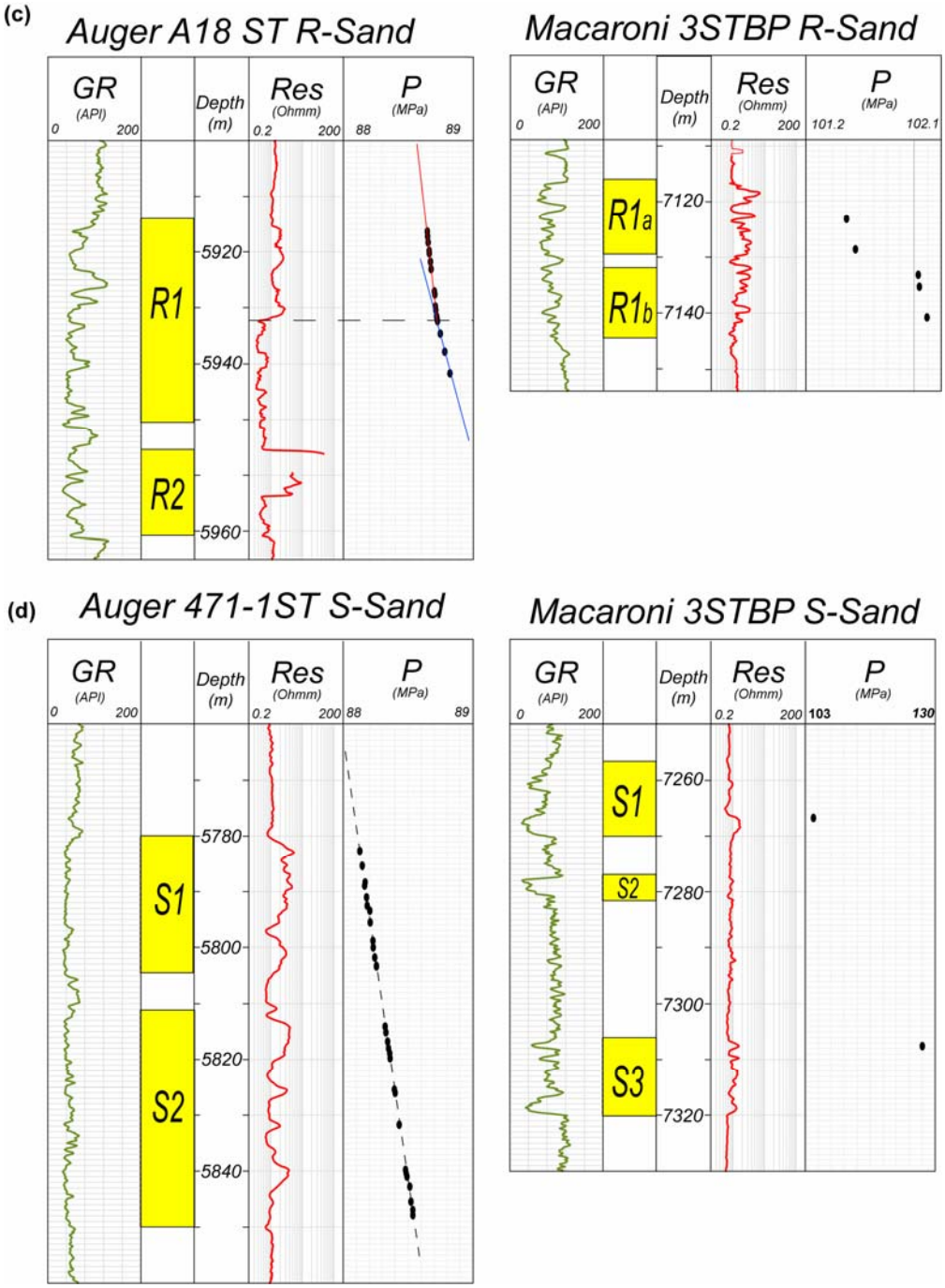

Figure **4-c**: Type log of the R sand at Auger and Macaroni. Note at the OWC there is a change in pressure gradients **d:** Type log of the S sand at Auger and Macaroni. Compared with Auger the S sand reservoir is thinner and has a lower net-to-gross at Macaroni.

Pressure and Stresses

In a passive margin setting, the overburden (σ_v) is generally assumed to be the maximum-principle stress; thus the least-principle stress is oriented horizontally and termed σ_h (Turcotte & Schubert, 1982). σ_v is estimated by integrating the bulk density from wireline density logs (*Appendix B*). Where no density data are available, the density data were extrapolated using Athy's Law (Athy, 1930) (*Appendix B*). There is an increase in water depth from 520 m at the vent location to 876 m at Auger to 1100m at Macaroni. This results in a decrease in overburden stress at any given depth of 4MPa at Auger and 6.4 MPa at Macaroni (Figure 5a) relative to the overburden stress at the vent site. The hydrostatic pressure gradient (P_h) in seawater was calculated by assuming an ocean water density of 1025kg/m^3 (a salinity of 35,000 ppm) (Figure 5a). The hydrostatic gradient in the sediment column was calculated using a pore water density of 1043.8kg/m^3 (equal to a salinity of 93,000 ppm at 75°C). This salinity data was taken from core reports of the O sand reservoir and was assumed throughout the sediment column. This results in a hydrostatic gradient of 10.229 MPa/km (0.45219 psi/ft) in the sediment column (Figure 5a).

The least principle stress (σ_h) is estimated from Leak-off tests (LOTs). LOTs or Pressure Integrity Tests (PITs) are performed routinely before drilling below a new casing shoe. In the case of an LOT, borehole pressure is raised until there is loss of fluid through the formation via fractures. In contrast in the case of a PIT, borehole pressure is raised to a pre-determined stress regardless of whether the formation is loosing fluid. The Leak-Off value is assumed to equal the least principle stress (σ_h)(Roegiers, 1989).

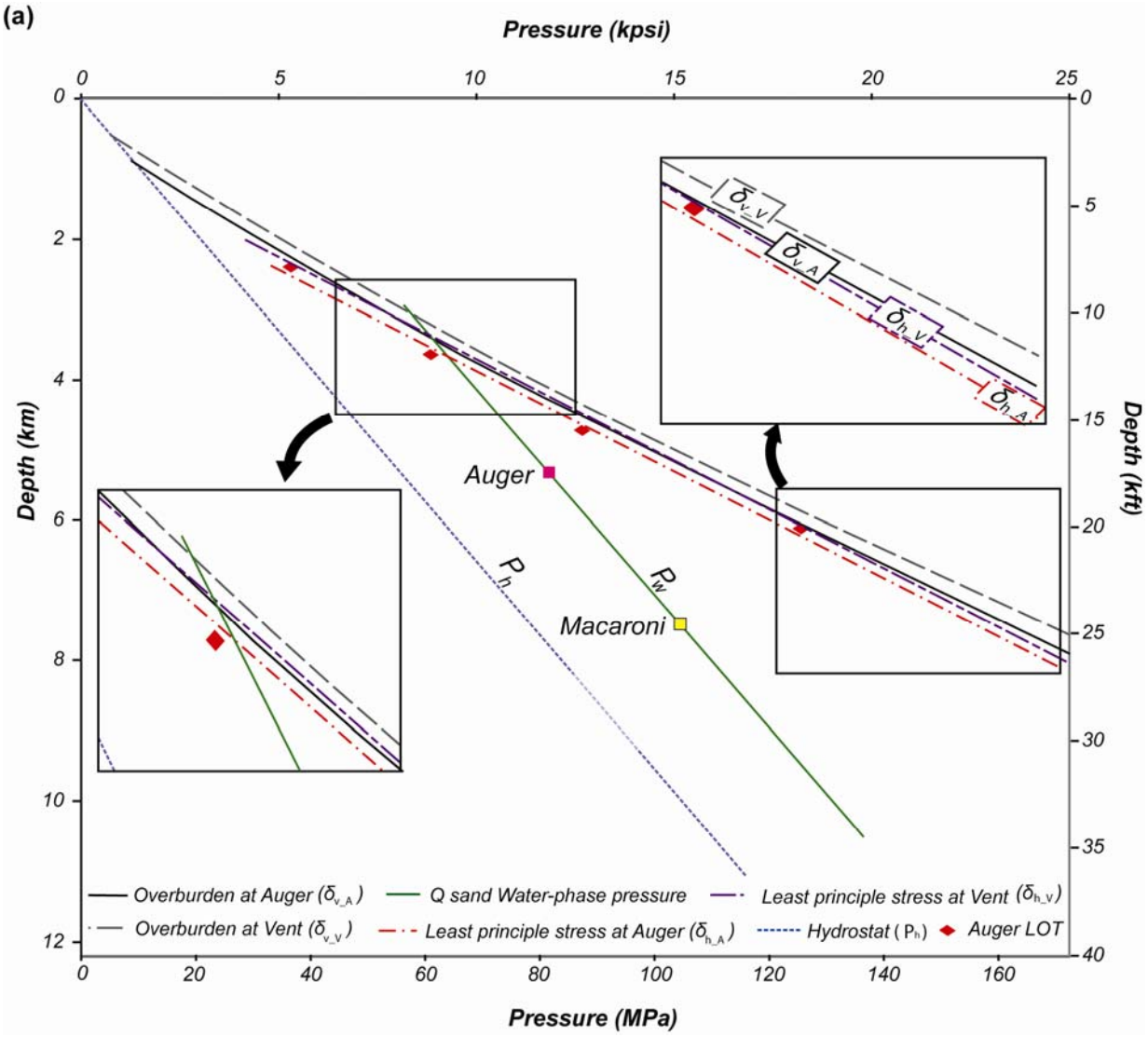

Figure **5a**: Pressures and Stresses in the Auger Basin. The hydrostatic pressure (P_h), overburden stress at Auger field (σ_{v_A}) and below the vent (σ_{v_V}), and the least principle stress at Auger (σ_{h_A}), and at the vent site (σ_{h_V}). The Q sand reservoir water-phase pressure (P_w) is plotted to illustrate the overpressured (P^*) nature of the minibasin aquifers.

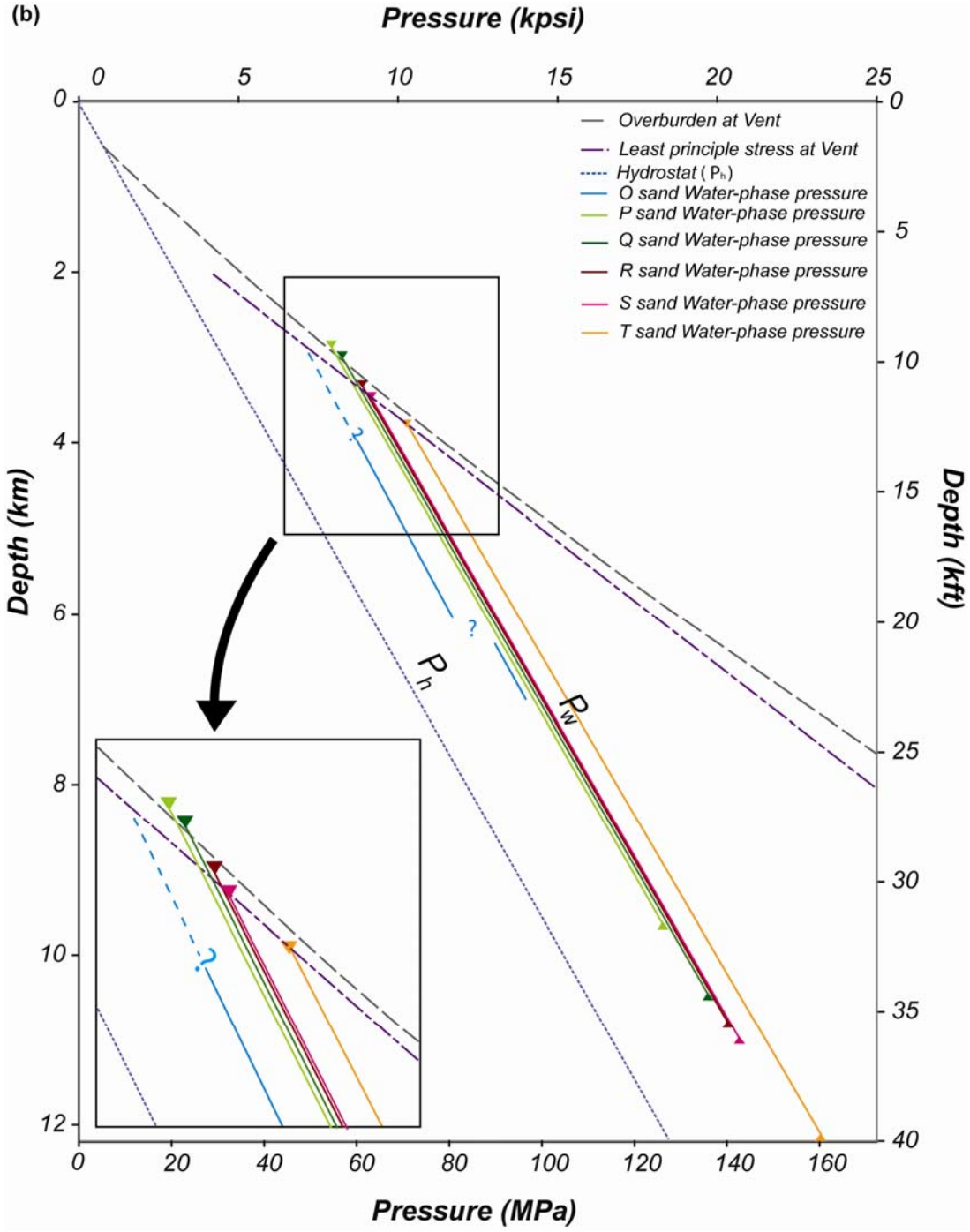

Figure **5b**: Reservoir pressures and principle stresses in the Auger Basin. The T, S, R, Q, P and O sand aquifer pressures (P_w) are plotted over their structural limits. Triangles represent the crests and bases of the sands. Pressures at the P and Q sand exceed the overburden at their crests. The R and S sand pore pressures exceed the least principle stresses at their crests. The pore pressures in the T sand do not appear to exceed the least principle stress at the crest of the sand, see text for discussion. The O sand does not have the same magnitude of over pressure at Auger and Macaroni.

I use only LOTs to analyze the least principle stress because it is a more accurate indicator of least principle stress (Roegiers, 1989). Unfortunately, while there were many PITs at Auger, only four LOTs were available (Figure 5a) (Table 3). I used a liner regression to interpolate the least principle stress between data points (Figure 5a). LOTs record a least principle stress (σ_h) that is 94.7% of the maximum principle stress (σ_v) (Figure 5a) (Table 3). Seldon (2005) and Lupa (2002) found similar behavior at Popeye ($\sigma_h / \sigma_v = 0.95$) and Bullwinkle Fields ($\sigma_h / \sigma_v = 0.975$), respectively (Table 3). LOTs were performed at Auger field and therefore represent the least principle stress at that location. To calculate the least principle stress at the vent locations I vertically shifted my linear regression of σ_h by 356m (1167ft) to account for the change in seafloor topography (Figure 5a).

Reservoir Pressures

I review the reservoir pressures for the Auger basin using the Q-sands as an example (data for the T, S, R, Q and P sands are found in Table 2 and Figure 5b). The Q-sand series has been well studied, is known to extend across the basin, and can be confidently mapped on 3D seismic (Booth *et al.*, 2000; Booth *et al.*, 2003).

I use Repeat Formation Tests (RFTs) to calculate pre-production formation pressures in both hydrocarbon and water phases at Auger, Cardamom and Macaroni (Figures 4, 6 and 7). Production began in 1994 at Auger, 1999 at Macaroni and in 2000 at Cardamom. Most RFT data points from Macaroni were taken in 1996. RFT measurements that were taken in the

hydrocarbon phase are extrapolated down the live hydrocarbon gradient (5.7MPa/km or 0.253psi/ft) to the Oil-Water Contact (OWC) as defined by seismic and/or well logs (Figure 6 and Figure 7b). At the OWC, the oil phase pressure (P_o) is assumed to equal the water phase pressure (P_w) (Figure 6 and Figure 7b). For this assumption to be correct the capillary entry pressure of the sand must be low, this is consistent with the 0.11Mpa (15psi) capillary entry pressure from core analysis. The water phase pressure is then extrapolated along the hydrostatic gradient away from well control; up to the sand crest and down the synclinal lows (Figure 6 and Figure 7b). This extrapolation is justified as sand permeabilities are high (400md).

The water phase overpressure:

$$P^* = P_w - P_h \qquad \textbf{Eq 1}$$

is used to characterize and compare the sandstone pressures as it is independent of depth (after Seldon and Flemings (2005)) (Figures 5 and 7).

The Q-sand at Auger has a P* of 27.97 MPa (4056psi), at Cardamom of 28.09 MPa (4074psi) and at Macaroni of 28.08 MPa (4071psi). A linear regression of the water-phase pressures at these three fields implies a fluid gradient of 10.292 MPa/km (0.455 psi/ft) (Figure 7b). This fluid gradient is only 0.063MPa/km (0.003psi/ft) higher than the fluid gradient calculated using sampled brine obtained from core data (10.229 MPa/km or 0.452 psi/ft). These results could signify that the pore water salinity used for calculation of the hydrostat is wrong and that the Q sand pore water salinity is actually 100,000ppm. This would imply that the sands follow the hydrostatic gradient and are therefore hydraulically connected. It is also possible that the measured pressure difference is driving fluid flow through the sand body.

The minor difference in fluid gradients of the Q sand aquifer pressures and the assumed hydrostat is extraordinary. Auger and Cardamom are separated by a salt ridge and a fault with ~600m of offset and thus effectively 16 km (10miles) (Figure 3), and Auger and Macaroni are separated by 19 km (12miles) (Figure 3). I believe this evidence suggest that the Q sand is one large connected sand body that is in pressure communication across the entire Auger Basin.

There is further evidence to suggest that the Q sand is a large hydraulically connected sand body. Firstly, the Q sand seismic event is a prominent feature on seismic, and easily mapable across the Auger Basin; this suggests that an acoustic impedance contrast exists across the basin. Secondly, reservoir simulations for the S sand required an area 53 times the volume of the field, roughly the entire basin, in order to support the observed rates (Kendrick, 1999). Thirdly, the stratigraphy of the Auger Basin is has been the focus of many studies, which have concluded that the lower sands of the Q are laterally extensive sheet sand deposits; my interpretation of the well logs is in agreement with previous authors (McGee *et al.*, 1993; Booth *et al.*, 2000; Booth *et al.*, 2003; Bohn *et al.*, 2008).

I extrapolate the overpressure along its observed pressure gradient over the entire depth that the sand is mapped (Figure 5b and Figure 8). At the crest, the pore pressures of the sand body exceed the least principle stresses of the overlying mudrocks (red colors, Figure 1b). I term this a 'leak point' e.g. Seldon and Flemings (2005) (Figure 8).

At a leak point the water phase pressure (P_w) converges on the least-principle stress (σ_h) and thus the horizontal effective stress ($\sigma'_h = \sigma_h - P_w$) is equal to zero. I propose that, at this

location, the Q sand pore pressure is hydraulically fracturing the surrounding mudrock and expelling fluid into the surrounding strata (Figure 5b and Figure 8).

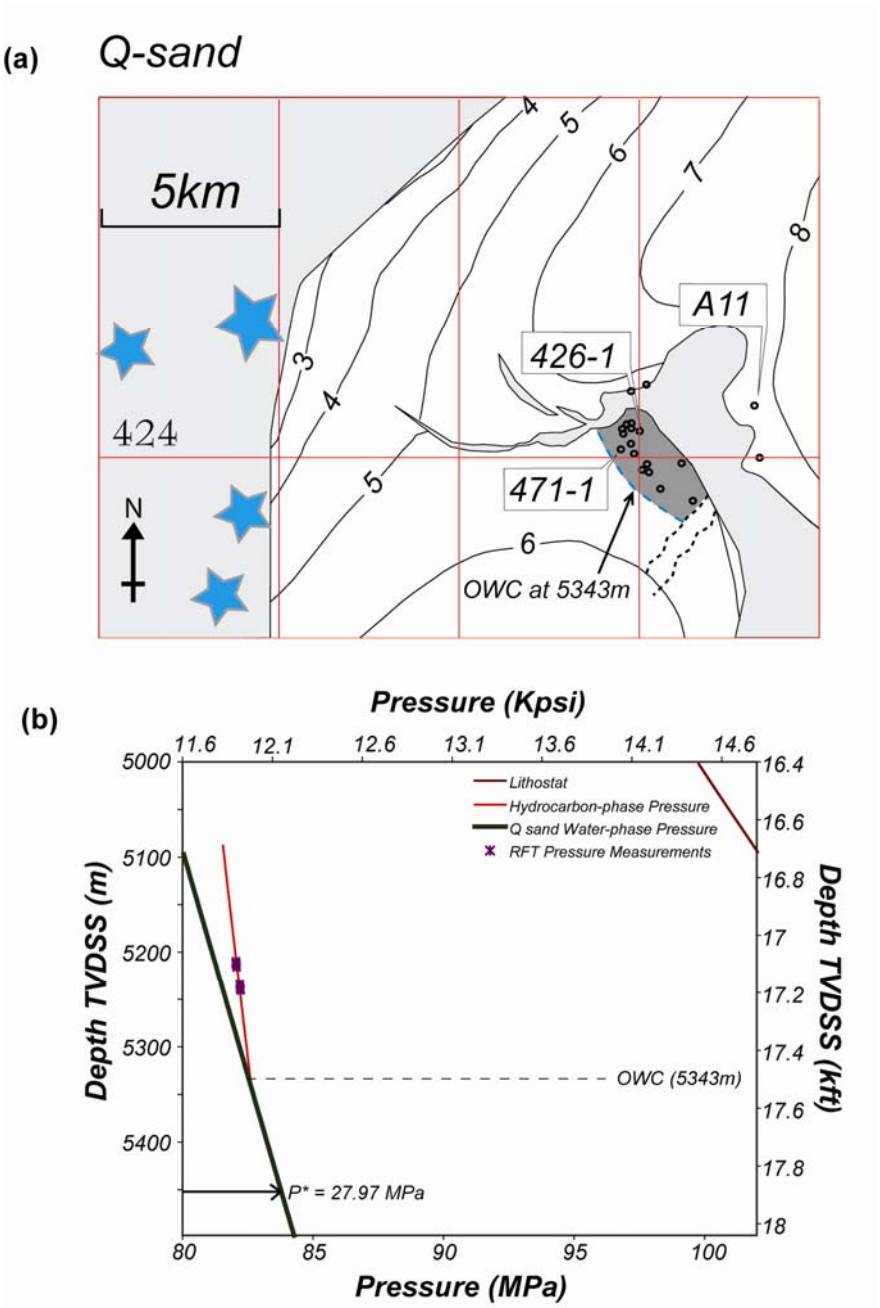

Figure **6-a**: Structure map of the Auger field at the Q horizon with the hydrocarbon saturated area delineated. Stars are the locations of vents at the seafloor. **b:** Pressure-depth plot illustrating the calculation of the of the water phase sand pressure when direct pressure measurements are in the hydrocarbon column.

I realize that there is potential error inherent in my depth conversion methodology (Appendix A). I have not accounted for any lateral velocity variation other than seafloor topography, and I have assumed that the sediment velocity varies linearly with the depth of my horizon. Table 1 gives a list of the sediment velocities used and shows the difference in the crestal height and pore pressure when using the interpolation method relative to using Auger sediment velocities.

I applied the same approach used in the Q sand to analyze the overpressures of the T, S, R, and P and O sands (Figure 5b).

The T sand (orange color, Figure 5b) is not penetrated at Macaroni. At Auger the T sand records the highest overpressure of the mapped sands (33.2 MPa). Because I only have data from a single field I cannot document that the pressures of the T sand lie along the hydrostatic gradient. However, if I extrapolate the overpressures recorded at Auger I find that pore pressures at the sand crest are well below the least principle stress (Figure 5b). This could result from the following issues. Firstly, I have no velocity data at macaroni and so could not use the velocity model in Appendix. Instead I use a constant sediment velocity from Auger. Depth conversion using a constant velocity generally under predicts sand structure relative to the interpolated velocity model (compare with Q sand Figure 8) (Table 1). Secondly, the T sand may simply not have enough structural relief for the pressures at the crest to exceed the least principle stress.

The S sand (pink colors Figure 5b and Figure 7d) records an overpressure of 28.17 MPa at Auger. There are only 2 pressure measurements at Macaroni and they record different overpressures (30.3 and 52.5 MPa) (Figure 4d and Figure 7d). The first pressure point is 30.3

MPa (4405psi), which is (2.13 MPa) greater than the overlying shallower sands. I interpret that this data point records the S sand overpressure and that the higher measurement is not correct. Structural mapping of the S sand and extrapolation of aquifer pressures to the crest suggests that at this location pore pressures exceed the least principle stresses (Figure 3 and Figure 5b).

The R sand (red-brown colors Figure 5 and Figure 7c) is overpressured by 28.07MPa at Auger and by 28.67 MPa at Macaroni. The RFT measurements from Auger are the only RFT measurements in my data set taken on the north side of the North Auger fault (A18, Figure 3). A linear regression of aquifer pressures equates to a fluid gradient of 10.56MPa/km (0.467psi/ft) which is 0.33MPa/km (0.015psi/ft) higher than the assumed hydrostatic gradient in the sediment column (Figure 7c). Although this is well within the tool window of accuracy, an increase in the pore water salinity to 130,000ppm could explain this discrepancy in fluid gradients or the pressure difference could be driving fluid flow through the sand. Pore pressures at the structural crest exceed the least principle stresses at the vent location (Figure 5)

The P sand (light-green colors, Figure 5 and Figure 7a) is overpressured by 27.81MPa at Auger and an overpressure of 27.99MPa at Macaroni. A linear regression of aquifer pressures equates to a fluid gradient of 10.31MPa/km (0.456psi/ft) which is only 0.09MPa/km (0.005psi/ft) higher than the measured hydrostatic gradient (Figure 7c). I interpret that the P sand at Auger is in communication with Macaroni. The pore pressures of the structural crest exceed the least principle stress and the overburden at the vent site (Figure 5). It is possible that the sediment velocities that were used at the sand crest may be too low. Similar to the Q sand even the sediment velocities calculated at Auger field put the crest of the sand and resulting pore pressures close to the least principle stress (Figure 8). I interpret that the P sand has a leak point at the sand crest.

The O sand (light-blue color, Figure 5) is overpressured by 22.31MPa at Auger and is overpressured by 28.44MPa at Macaroni. The O sand, a channelized deposit, has limited structural relief, poor seismic continuity (Figure 2) and a has been interpreted as having a lesser aerial extent than the deeper sands (McGee *et al.*, 1993; Booth *et al.*, 2000; Booth *et al.*, 2003; Bohn *et al.*, 2008). I would, therefore, not expect to see similar overpressures at Auger and Macaroni. The O sand is also very difficult to map across the basin and to determine the structural crest (dashed blue line Figure 2 and Figure 5b). I interpret that the O sand is not in pressure communication across the basin. The O sand pressures at Auger may be constrained by a leak point but I have no definitive data to suggest this.

The overpressures of the S, R, Q and P sands are successively less (Table 2) (Figure 5b). The crests of the S, R, Q and P sands reach successively higher levels (Figure 3 and Figure 5b) (Table 2). Despite the potential discrepancies in my depth conversion I suggest that the pressures reached at the crests of the S, R, Q, P-sands are elevated enough to induce fluid expulsion and create a minibasin leak point. I interpret that the difference in crestal height controls sand pressures.

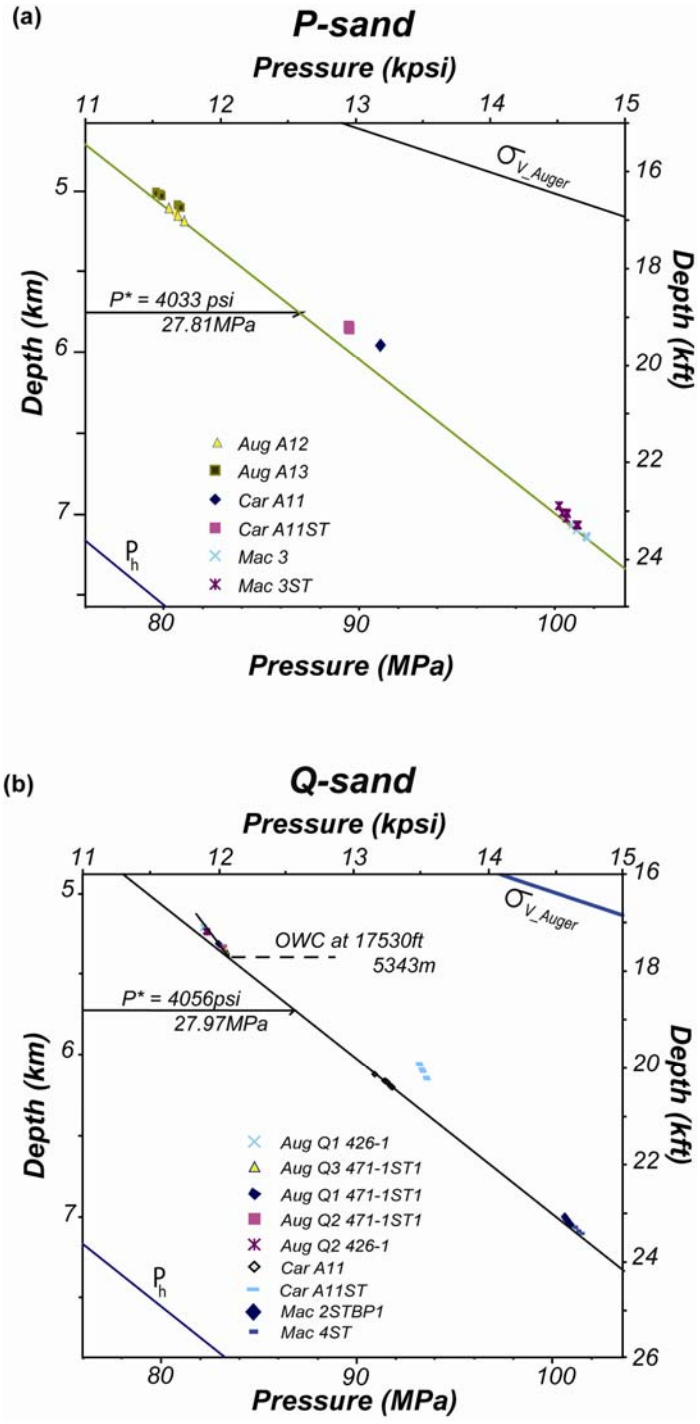

Figure **7-a**: Reservoir pressures of the P sand. **b:** Reservoir pressures of the Q sand. Water-phase pressures are extrapolated along the hydrostatic gradient and show that sands at Auger and Macaroni have nearly the same value of overpressure.

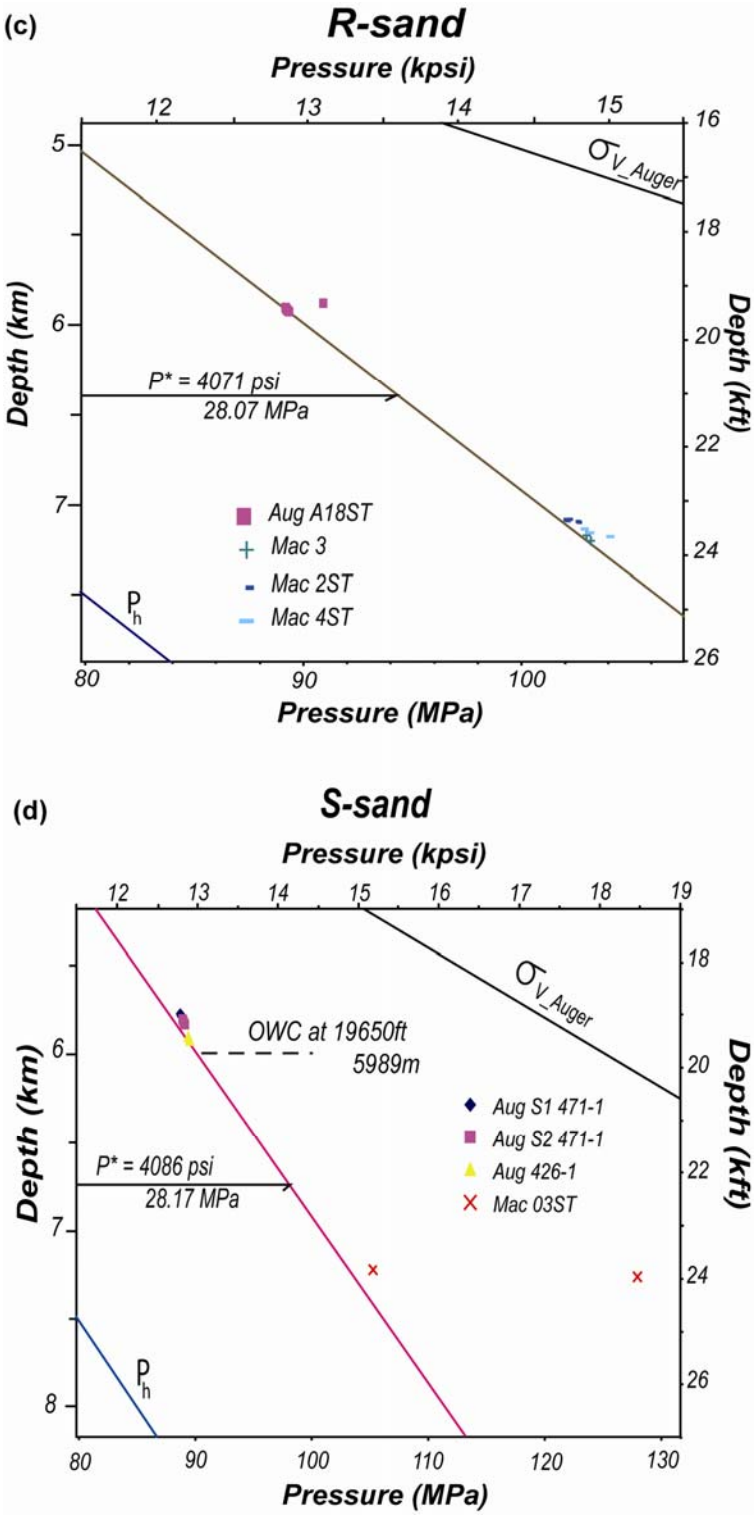

Figure **7c**: Reservoir pressures of the R sand. **d:** Reservoir pressures of the S sand.

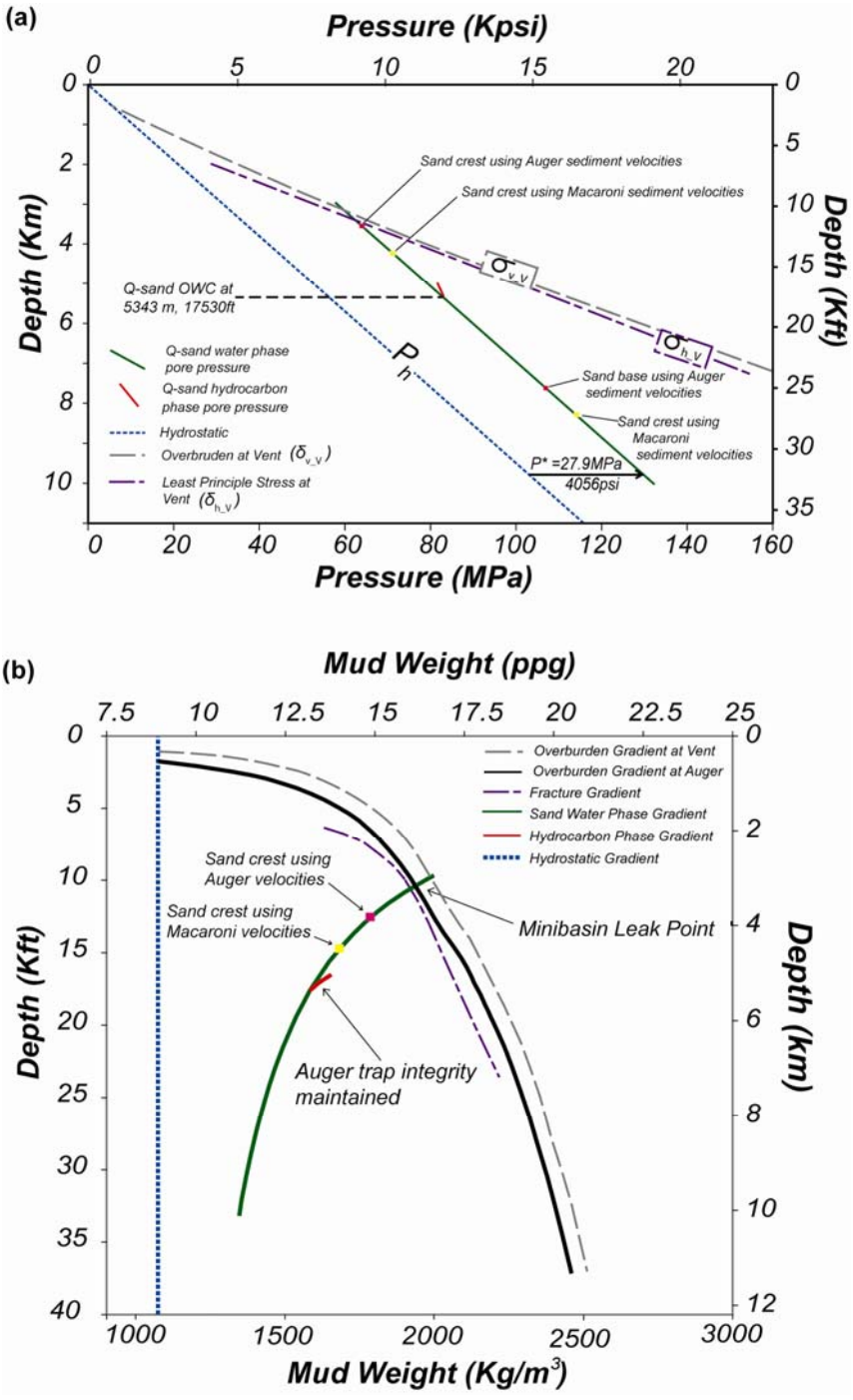

Figure **8-a**: Basin scale pressure-depth plot of the Q sand illustrating the convergence of the sand crest pore pressures to the overburden at the vent site. **b:** Fluid pressure gradient plot of the Q sand. This type of plot is typically used by drilling engineers to calculate the mud weight used during drilling. Both plots show the effect of different sediment velocities on the sand crest height and therefore sand crest pressure.

The Seafloor Vent Complex

Eight cone-shaped mounds, located along the northwest flank of the Auger minibasin, are interpreted to be mud volcanoes (Figures 1, 9 and 10). Seven of these mud volcanoes lie directly along the flank of the basin in blocks 424 and 468 (#1-#7, Figure 9), and one lies approximately 5 km further west within the upraised flank (#8, Figure 9). The vents range in size; the largest (#1, Figure 9) at 1170m (3840ft) in diameter and ~30m (~100ft) high, the other vents are similar to each other in size and are ~840m (~2750ft) in diameter and 50-75ft (15- 23m) high. There is a long normal fault that runs along the flank of Vents 3-7 and intersects with a second basin fault that runs along the southern edge of Vents 1-2 (Fig. 10a). Vent 8 is on the western side of the tabular salt body and may not be directly tied to the sands in Auger Basin.

The mud volcanoes have flat tops and negative seismic amplitudes that record a decrease in impedance at the water-seafloor interface (blue colors, Fig. 9). The negative seismic amplitudes may result from the free gas and liquid mud present at the craters of the mud volcanoes described by Macdonald (2000) and Kohl and Roberts (1994).

A series of flow-like features, oriented down the topographic gradient, emanate from the mud volcanoes (Figures 9, 10a, 10b). These features have positive seismic amplitudes that are more positive than the adjacent, undeformed, seafloor (Figure 9 and Figure 10). The higher amplitude response of some flows may be caused by a greater degree of consolidation caused by deposition as a debris flow (Seldon & Flemings, 2005). The flows from Vents 1 and 4 have a total area of 15km² and 10km² respectively.

The leak points of the S, R, Q, P sands are overlain by a series of cylindrical GWZ (Figure 2 and Figure 10). At the seafloor, directly above these GWZ's, is the Auger Vent Suite. GWZ's are

sub-surface feeder systems beneath seafloor vents, in which fluid travels upwards from the source to the expulsion point. The chaotic seismic signature of GWZ's may result from fluids destroying depositional layering, as they travel upwards and thus removing any acoustic impedance contrasts that may have existed (Kohl & Roberts, 1994; Graue, 2000). Expelled gasses may also become trapped in small pockets further compounding the problem with seismic imaging (Graue, 2000). Seismic horizons decrease in amplitude and become increasingly harder to image with closer proximity to the GWZ (Figure 2 and Figure 10c). This presents a challenge when mapping horizons with structural crests that reach the GWZ. Beneath Vent #4 the GWZ is, in sections, over 2km wide and many horizons fade into it (Figure 10c).

The geometry and location of the reservoir sand's structural crest changes from the S to the P sand. The P and Q sands have structural crests in GB 424, underneath Vent 4 (Figure 3). Whereas the S and R sands have a much broader crest with high points in GB 381 and 382, directly below Vent 1 (Figure 3). I conjecture that the deeper sands in Auger basin are fueling venting in blocks GB 381 and 382 and that the shallower sands Q and P are fueling venting in blocks GB 424 and 468.

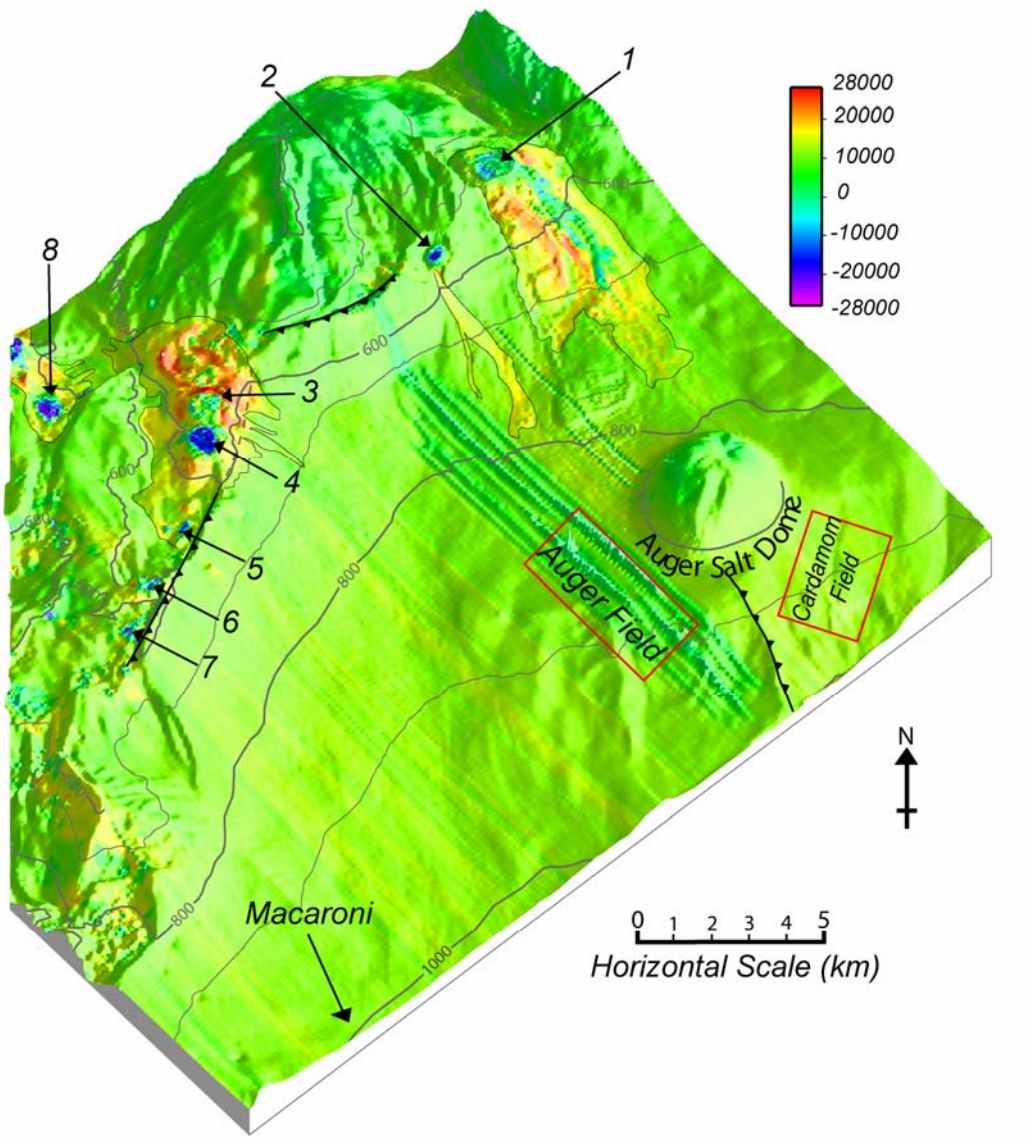

Figure **9**: 3D Amplitude extraction map of the seafloor with depth contours. Flows can be seen emanating from mud volcanoes (reds and yellows). The locations of the mud volcanoes are numbered. Notice a decrease in amplitude (blues) at the flat tops of the mud volcanoes, this may be due to free gas or liquid at the crater . Contour interval is 100m.

The vents appear to have been long-lived. To illustrate this I compare seismic amplitudes at the seafloor (Figure 9) with those 16 ms and 56 ms below the seafloor (Figure 10a and Figure 10b). At the seafloor, mud volcanoes and associated flows are clearly imaged. At 16 ms below the seafloor, Mud volcano #1 is imaged, but flows associated with the other volcanoes are not. However, at 16 ms, the zone of low seismic amplitude labeled as the gas wipe out zone (GWZ, Figure 10c) is present. The GWZ follows the trend of faulting. At 56 ms below the seafloor a preceding episode of expulsion can be imaged; the expulsion of fluid and sediments has been a dominant feature of seafloor topography through time (Figure 10b). In Figure 10c, a much deeper mud volcano is interpreted; the same GWZ descends to the crests of the S, R Q and P sands (~400 ms).

Kohl and Roberts (1994) explored Vent 1 with manned submersibles (Figure 9). They observed expulsion of methane and mud venting and found that 65% of the foraminifera recovered were of Miocene age. They interpreted that pressurized fluids entrained clays from depth. The age of the flows is unknown, however, based on substantial thinning of high sealevel-stand hemipelagic sediment across the uppermost flows that emanate from Vent 1, (Roberts & Carney, 1997) reasoned that the mudflows most likely post-date the sea level lowstand at 17ka. Macdonald et al (2000) placed a temperature probe in the mudlake of Vent 4 and used satellite imagery to track slicks created from eruption events. Rapidly fluctuating temperatures coincided with the occurrence of large oil slicks in the area. Macdonald et al (2000) interpreted from the magnitude of the temperature fluctuations that the fluids released during the study must have originated from at least 2310m (7575ft) beneath the seafloor (MacDonald *et al.*, 2000), which is approximately the depth of the P sand crest (Fig. 5). Aharon (2003) found long chained

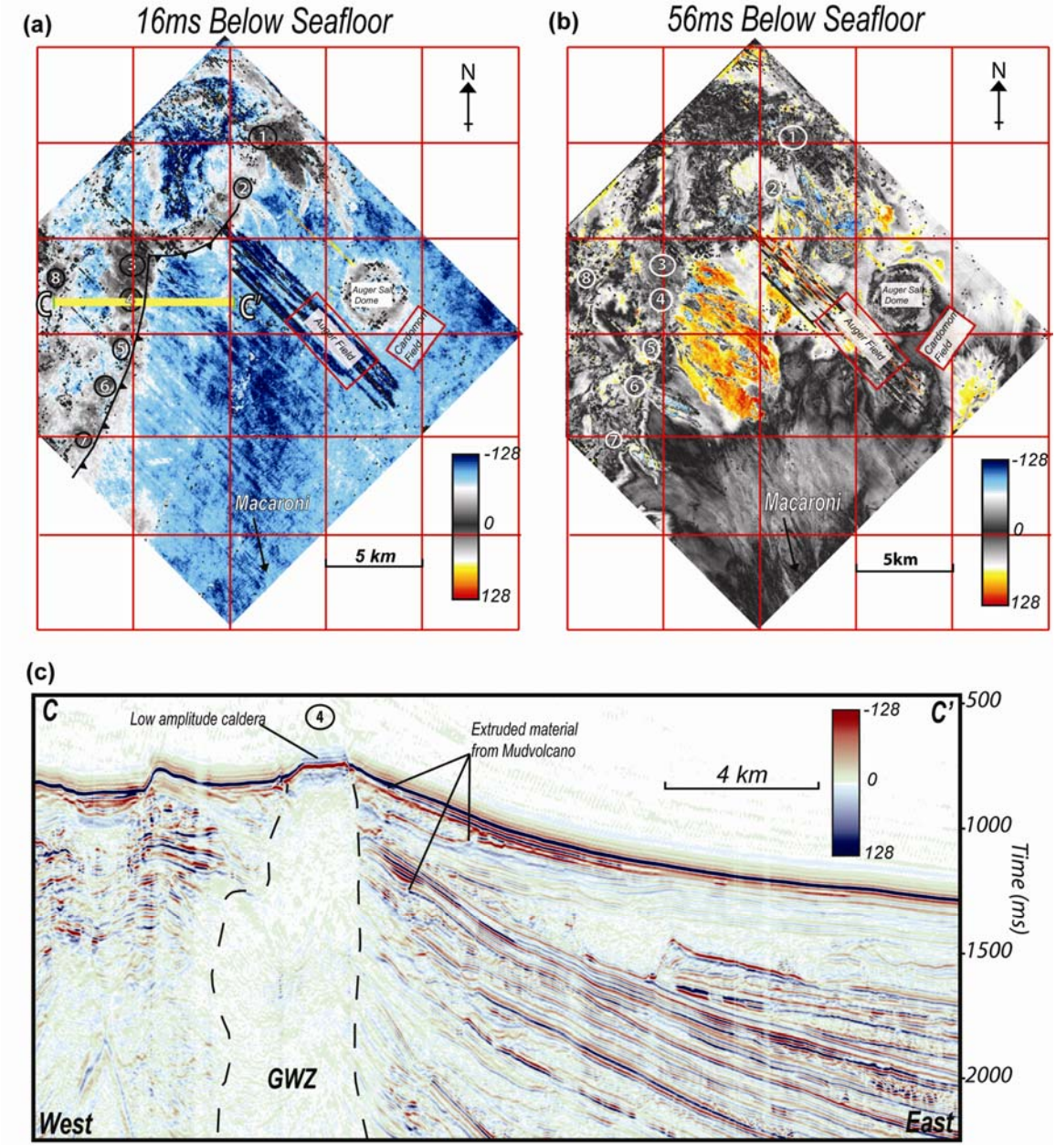

Figure **10-a**: Flattened time slice at 16ms below the seafloor illustrating how GWZ of the mud volcanoes 3-7 merge. The tops of previous flows from mud volcanoes 1 and 2 are also be imaged. **b:** Flattened time slice 56ms below the seafloor which shows a multitude of previous flows from mud volcanoes 3-7 that have flown down the flank of the basin towards Macaroni. **c:** Shallow time cross section of mud volcano 4 showing previous extruded flows and the large vertical section of chaotic reflectors in the GWZ beneath the mud volcanoes.

hydrocarbons at the mud volcanoes that match the 2% of high alkane (<C11) fingerprint of produced hydrocarbons at Auger field.

Discussion

My data shows that a sand body with good lithologic connectivity can be in pressure communication over km scale distances. In the Auger basin a regression of water phase pressures from three separate locations results in a near perfect correlation with the measured hydrostatic gradient (+/- 0.063MPa/km) (Figure 7). I believe I have documented pressure connectivity in the S, R, Q and P sands over nearly 20km (Figures 1, 5 and 7). My data set shows that at three separate locations and depths the S, R, Q and P sand pressures follow the hydrostatic gradient and have the nearly same magnitude of overpressure at each locality (+/- 0.6MPa) (Figure 7).

The pore pressures at the structural crests of the S, R, Q and P sands exceed the least principle stresses of the overlying strata (Figure 5b and Figure 8). When fluid pressures in the crests of the overpressured sand bodies exceed the least principle stress, permeability is self-generating and fluids are expelled, I term this a 'leak point' (Figure 8). I interpret that this expulsion constrains the pore pressures of the sands and maintains the integrity of the hydrocarbon traps at Auger and Macaroni Field (Figure 8). Essentially, at the crest of the sands, the overlying shales act as a pressure valve for the sand; when sand body pressures increase fractures dilate and the pressure is 'vented off', this venting eventually decreases the pressure and the fractures close.

I propose that the leak points of the S, R, Q, and P sands contribute to the fluid and material expelled by the mud volcanoes at the seafloor. The leak points of the S, R, Q, P sands

are overlain by a series of cylindrical Gas Wipe-out Zones consisting of chaotic low amplitude reflectors (Figure 2 and Figure 10). At the seafloor, directly above these GWZ's, lies the Auger Vent Suite. I suggest that the elevated pore pressures at the crest of these sands are inducing hydraulic fractures in the overlying mudrocks and causing a significant volume of fluid to be expelled (Figures 8, 9 and 10). The resulting fractures can then propagate for hundreds of meters above the overpressured source, allowing the expelled fluids to form 'fluidization pipes' or 'diatremes' as they travel upwards and form mud volcanoes at the seafloor (Stewart & Davies, 2006).

An apparent difference in mud volcano processes in the Auger Basin compared to those studied in the South Caspian Basin is the source of the expelled mud. Mud Volcanoes in the South Caspian are sourced by a single overpressured layer of mud, extruded like magma into the overlying sediments (Stewart & Davies, 2006). At the Auger Basin I suggest that overpressured fluids from a multitude of sources, including but not limited to the S, R, Q and P sands that feed the diatreme system and the fluids entrain muds during transport to the seafloor (Figure 2 and Figure 10c).

The O and N sands are present in Macaroni and Oregano respectively, but do not have similar values of P* (Figure 5b). I suggest that O and N sands do not communicate across the basin as the sands are not as aerially extensive or are bisected by erosional channels. This is consistent with the findings of Bohn et al. (2008) who found that irregular GWC movement most likely resulted in poor aquifer support to the South and East of Auger Field (Bohn et al., 2008). The O and N sands also contain erosional channel sequences filled with low net to gross, low permeability muds, and sands which are not in pressure communication with the rest of the reservoir sands which may further compartmentalize the sand bodies (Bohn et al., 2008). The T

sands are at a significantly higher pressure than the S sands. I believe the reason for this is the limited structural relief of the T sand.

My data suggest that the overpressure at Macaroni is slightly higher than at Auger in the S, R, Q and P sands (Table 2 and Figure 7). This may record the pressure gradient driving flow upward through the sands. In the Q sand, the Macaroni overpressure is 0.09MPa higher than at Auger , which results in a vertical overpressure gradient of 61 Pa/m. Assuming a sandstone permeability of 400 md ($3.94x10^{-13}$ m^2), this equates to a flux through the Q of $7.7x10^{-7}$ m^2 /s (Appendix C). An alternative interpretation is that the apparent overpressure between Auger and Macaroni in the Q sand is present because the pore fluid is denser than I have assumed. An increase in 7000 ppm in pore water salinity, from the 93,000 ppm I have assumed, to 100,000 ppm would account for the pressure difference observed.

In Appendix C, I also estimated the flux draining the mudstones bounding the Q. Assuming a mudstone permeability of $1x10^{-19}$, the fluid flux through the Q sand would be $5.4x10^{-8}$ m^2/s. This flux is 14 times less than I calculated for flow through the Q sand. To generate a flux of $7.7x10^{-7}$, the permeability of the mudrocks must increase by 10 times ($1x10^{-18}$).

The Lusi mud volcano represents a rare glimpse at the processes behind subsurface fluid flow in action, on land and with direct pressure measurements (Davies *et al.*, 2007; Davies *et al.*, 2008). In under two years Lusi has expelled 5000-180,000m^3 of fluid and mud, covering an area over 7km^2 and causing $420 million in damages (Tingay *et al.*, 2008). Lusi was caused by the artificial generation of a fluid pathway between a deeper formation of higher pressure and a shallower formation of lower pressure (Davies *et al.*, 2008; Tingay *et al.*, 2008).

In Figure 8b, I have re-plotted the pressure field as a function of gradient vs. depth. This portrayal of the pressure field is commonly used by drilling engineers to visualize the minimum fluid density that must be in the borehole when an overpressured horizon is drilled. Specifically, if a well were drilled at the peak of the structure, a mud weight of 16 lb/gal (1917 kg/m^3) would be necessary to hold back the fluid pressure. However, this mud weight is also equal to the least principle stress and lost circulation would result.

Davies et al. (2008) describe how at the Lusi mud volcano, drillers inadvertently drilled into an overpressured zone with a low mudweight. The result was that severely overpressured fluids moved up through the open borehole to shallower depths. Ultimately those overpressured fluids exceeded the least horizontal stress and self fractured to the surface. The Auger sands drive a mud volcano driven by natural processes. However, the underlying process is exactly what drives Lusi today. At Auger, the most recent expelled material, defined by higher amplitudes, from vents 1 and 4 has covered an area of 15 km² and 10 km² respectively and may be a sign of things to come for Lusi (Figure 9).

The greatest cause of uncertainty in this study is the conversion of seismic data from time to depth (Appendix A). The nearest velocity control point to the Vent site is Auger Field. At the sand crest, the interpolated velocities are ~600m/s lower than the sediment velocities calculated at Auger (Table 1). If the sediment velocity derived from Auger is used to depth convert the sand horizons the crests of the S, R, Q, P sands are 765m, 826m, 1018m, 1138m deeper, respectively (Table 1 and Figure 8).

I believe I am justified to use a sediment velocity lower than those derived at Auger. Sediments compact and become denser the deeper they are buried. Therefore, one would expect

that shallower sediments would have lower sediment velocities. The sediment column above the vent site is 446ms less than Auger and would therefore have slower sediment velocities. To account for this change in sediment velocity I used a linear extrapolation of velocity with depth using the two reference locations Auger and Macaroni (Appendix A). Although I understand that more complex depth conversion methods exist I believe my depth conversion method to be adequate for the purposes of this study.

I am very confident in my pressure correlations from Auger to Macaroni field in R, Q and P sands. I also believe the S sand is in pressure connection across the basin. Although the S-sand does not have a perfect correlation (+/-2MPa) with Macaroni RFT measurements; this is most likely due to the small number of samples taken, and the possibility that the tool was beginning to fail, as is evidenced by later erratic measurements (Figure 7).

The ability to constrain pore pressures in a sand body has important implications for prospective reservoir targets, especially those in basins where seafloor venting is evident. Sand pressures and trap integrities can be estimated without direct pressure measurements by reverse extrapolation. Furthermore, with minimal pressure measurements one can predict pressures across km scale distances as long as there is a good understanding of the stratigraphic framework and sand connectivity. This could greatly aid the design of an effective and safe drilling program.

Conclusions

The pore pressures of the S, R, Q and P sands are constrained by fluid expulsion at the seafloor and thus hydrocarbon trap integrities at Auger and Macaroni Fields are protected. The pore pressures of the S, R, Q and P sands can be extrapolated down the hydrostatic gradient

across the basin and are in pressure communication. The S, R, Q and P sands have the same value of P*. The bases of the sands are underpressured relative to their surrounding mudrocks, whereas at the structural crests of the sands the pore pressures are high enough to induce fracturing in the overlying cap rocks and expel fluids. The expelled fluids contribute to the mud and fluid venting at the seafloor.

Tables

Table 1: Effect of Sediment velocity on crest height

Sand	OWT from Seafloor to horizon at Auger (s)	OWT from Seafloor to horizon at Macaroni (s)	OWT from Seafloor to horizon at Vent (s)	Depth to sand at Auger (mbsf)	Depth to sand at Macaroni (mbsf)	Auger sediment velocity (m/s)	Macaroni sediment velocity (m/s)	Model sediment velocity at crest (m/s)	Depth to crest (mbsf) (Auger velocities)	Depth to crest (mbsf) (modeled velocities)
O	1.7994	1.864	-	3985	4671	2214	2506	-		
P	1.8278	2.107	1.357	4132	5460	2260	2580	1695	3066	2301
Q	1.9206	2.153	1.402	4407	5932	2294	2755	1704	3216	2390
R	2.021	2.252	1.620	4672	5997	2312	2683	1683	3745	2727
S	2.099	2.453	1.692	4904	6152	2366	2508	1691	4003	2862
T	2.101	-	1.755	5054	-	2404	-	-	4220	-

Table 2: Principle stresses in relation to sand structure

Sand	Location	P*	Depth to HWC (mbsf)	Pw at HWC (MPa)	Sand base (mbsf)	Pw at base (MPa	Sand crest (mbsf)	Pw at crest (MPa)	σ_v at crest (MPA	σ_h at crest (MPa)
O	Auger	20.9	4062	72.8	6968	-	-	-	-	-
	Macaroni	28.6	6848	92.9						
P	Auger	27.83	4312	80.8	8450	126.5	2301	56.4	53.2	49.1
	Macaroni	27.99	7010	99.5						
Q	Auger	27.97	4414	82.8	9300	135.4	2390	55.9	55.2	51.3
	Macaroni	28.06	7106	100.66						
R	Auger	28.07	4640	84.3	9600	138.5	2727	60.9	62.5	59.4
	Macaroni	28.67	7218	102.4						
S	Auger	28.17	5113	89.25	9800	140.6	2862	62.4	65.5	62.4
	Macaroni	30.3	7266	104.7						
T	Auger	32.0	5966	33.3	10800	159.7	4220	76.1	84.2	80.7

Table 3: Leak-off Test data summary

TVDSS of LOT (m)	**LOT (MPa)**	**σ_v (MPa)**	**LOT/ σ_v**
2400	36.25	39.9	0.908
3741	64.4	68.9	0.935
4720	87.2	93.06	0.937
6101	125.3	127.3	0.984

Table **4**: Nomenclature table

Variable	Description	Dimensions*
dt	Time from Reference Point	T
dZ	Difference in depth	L
g	Gravitational Acceleration	LT^{-1}
h	Thickness of sand body	L
k	Permeability	L^2
l	Length of Auger Basin	L
q	Fluid flux through sand body	L^2T^{-1}
u	Porepressure	$ML^{-1}T^{-2}$
LOT	Leak-off Test	-
OWT	Seismic one-way travel time	T
P_h	Hydrostatic Pressure	$ML^{-1}T^{-2}$
P_o	Oil-phase Pressure	$ML^{-1}T^{-2}$
P_w	Water-phase Pressure	$ML^{-1}T^{-2}$
$P*$	Overpressure	$ML^{-1}T^{-2}$
$dP*$	Difference in Overpressure	$ML^{-1}T^{-2}$
RFT	Repeat Formation Test	-
TVDSS	True Vertical Depth Sub-Sea	L
V_a	Sediment velocity at Auger	LT^{-1}
V_m	Sediment velocity at Macaroni	LT^{-1}
V_{sw}	Velocity of sound in seawater	LT^{-1}
V_z	Sediment velocity	LT^{-1}
Z	Depth	L
Z_h	Depth to horizon	
Z_{sf}	Depth to Seafloor	L
β	Compressibility Constant	$M^{-1}LT^{-2}$
$\lambda*$	Overburden Ratio	-
μ	Voscocity	ML^2
ρ_b	Bulk Density	ML^{-3}
ρ_f	Fluid Density	ML^{-3}
ρ_{ma}	Matrix Density (assumed to be 2.65 g/cm)	ML^{-3}
σ_h	Minimum horizontal stress (assumed to equal Least Principle Stress)	$ML^{-1}T^{-2}$
σ_{h_A}	Minimum Principle Stress at Auger field	$ML^{-1}T^{-2}$
σ_{h_M}	Minimum Principle Stress at Macaroni field	$ML^{-1}T^{-2}$

σ_{h_V}	Minimum Principle Stress at Vent	$ML^{-1}T^{-2}$
σ'_h	Minimum Horizontal Effective Stress	$ML^{-1}T^{-2}$
σ_v	Overburden Stress or Maximum Principle Stress	$ML^{-1}T^{-2}$
σ_{v_A}	Maximum Principle Stress at Auger Field	$ML^{-1}T^{-2}$
σ_{v_M}	Maximum Principle Stress at Macaroni Field	$ML^{-1}T^{-2}$
σ_{v_V}	Maximum Principle Stress below seafloor vents	$ML^{-1}T^{-2}$
ϕ	Porosity	
ϕ_0	Reference Porosity	
ΔT	Macaroni Field time – Auger Field time	T
ΔV	Difference in Velocity	LT^{-1}

Appendix A

Depth Conversion Velocity Model

I use a simple two layer velocity model in order to account for the variation in seafloor topography.

$$Z = \left[V_z \left(Z_h - Z_{Sf} \right) \right] + \left[V_{sw} \cdot Z_{Sf} \right] \quad \textbf{A1}$$

Where: Z is the depth, V_z is the sediment velocity (see Eq A2), Z_h is the depth to the horizon, Z_{Sf} is the depth to the seafloor and V_{sw} is the speed of sound in seawater ($1500 ms^{-1}$).

The effective stress in Macaroni is greater, causing greater compaction of the sediments. This causes sediment velocities to be faster at Macaroni Field than those at Auger Field.

To account for this variation in velocity, I linearly interpolate the velocities with depth across the field using the Auger Field velocities as my control point.

The interpolation method is:

$$V_z = V_a + \Delta V \cdot \left(\frac{dt}{\Delta T} \right) \quad \textbf{A2}$$

Where: V_z is the sediment velocity at any given depth, V_a is the sediment velocity at Auger Field, ΔV is the difference in sediment velocities between Auger and Macaroni, dt is the difference in time from Auger Field measured at well 471-1ST (Figure 6) and ΔT is the total difference in time from Auger to Macaroni Field (Figure A1).

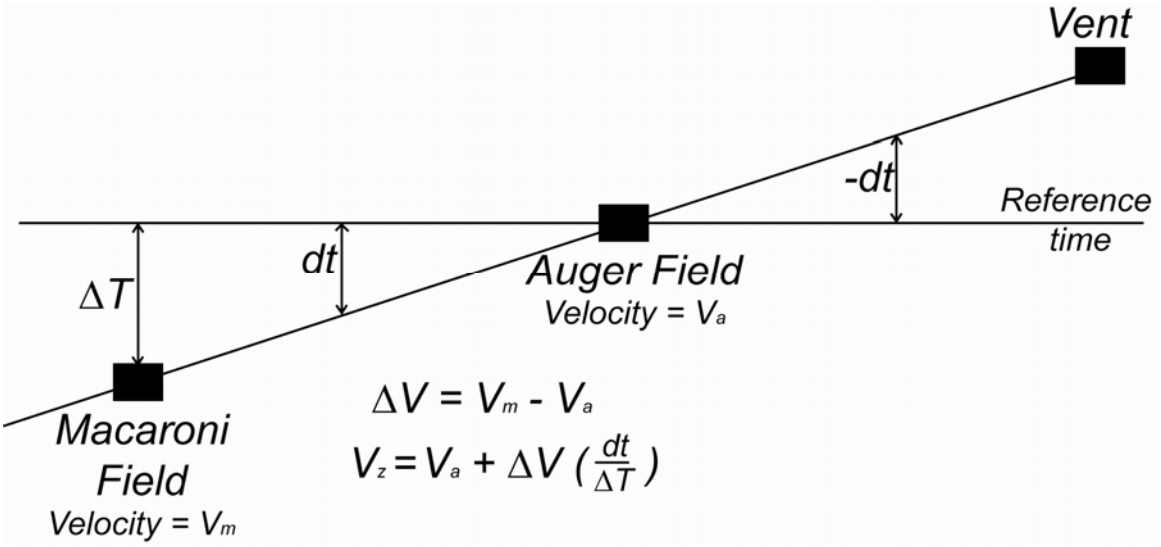

Figure **11**: Depth conversion velocity model

Appendix B

Estimation of Overburden Stresses

σ_v was estimated only at Auger. In this location, there were no measurements of bulk density from the seafloor to a depth of 1500m (4925ft) below the sea floor (Fig. A-1). The following approach was used to estimate the overburden stress.

Porosity (ϕ) was calculated from the density log:

$$\phi = \frac{\rho_{ma} - \rho_b}{\rho_{ma} - \rho_f} \qquad \textbf{B1}$$

A matrix density (ρ_{ma}) of 2.65g/cc and a fluid density of 1.15 g/cc were assumed. A least squares regression of these data on a semi-log plot over the interval from 1500-4500 mbsf was then used to calculate phi0 and Beta in Athy's(1930) law:

$$\phi = \phi_0 e^{-\beta z} \qquad \textbf{B2}$$

I find ϕ_0 and β to be 0.4265 and 0.002 respectively. Equation B1 was rearranged to solve for ρ_b given ϕ. These bulk density measurements were then used to fill in the gaps above the recorded wireline density measurements (Figure 12).

Bulk density measurements then integrated from the seafloor at 0 to the depth below seafloor at z, to calculate the vertical stress from the mudline according to Eq. B3.

$$\sigma_v = g\int_0^z \rho_b dz \qquad \textbf{B3}$$

To estimate overburden stresses at the vent site, where there are no well penetrations, the 360m change in seafloor topography must be accounted for. The overburden stress calculated at Auger was therefore vertically shifted upwards by 360m to estimate the overburden at the vent site.

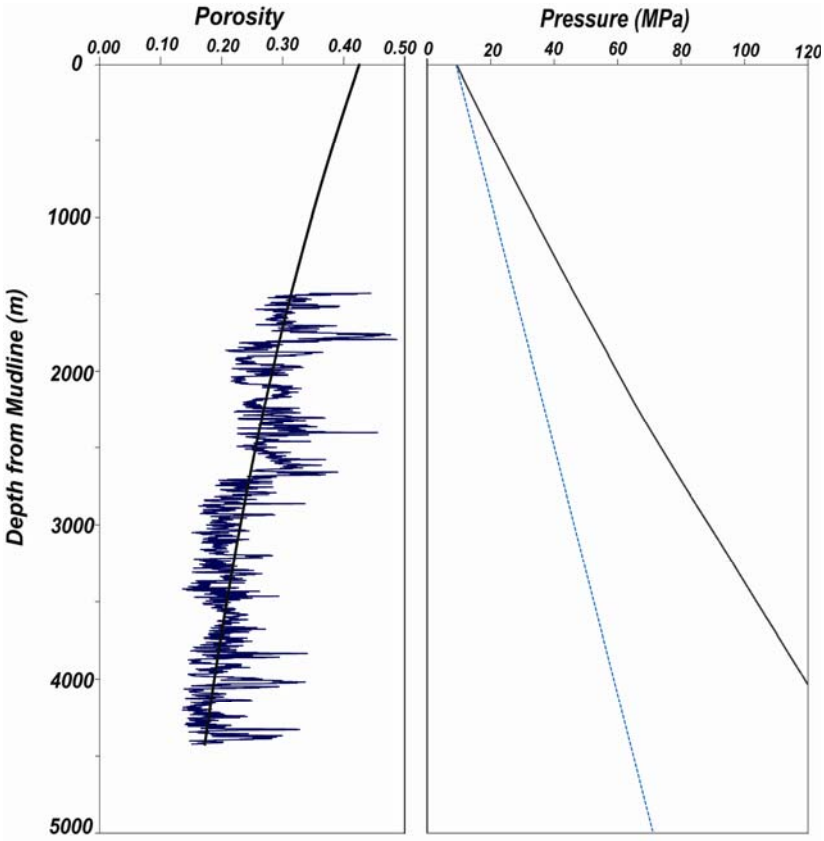

Figure **12**: Calculation of overburden. An exponential regression of porosity data is used to estimate the overburden stress where no depth data is available. Porosity data is used to calculate bulk density which is then integrated. The resulting overburden curve (black line) is shown on the second plot.

Appendix C

Calculation of Fluid Flux through a Sand Body

If I consider darcy flow that is steady and mudstone properties are homogeneous and isotropic flow, though a mudstone can be expressed as:

$$\nabla^2 P^* = 0 \qquad \textbf{C1}$$

Eq C1 was solved analytically by Philips (1991) for a thin straight permeable body, long relative to its width, encased in low permeability mudrock and with a permeability greater than the surrounding mudrock. Flow is steady and unidirectional far from the permeable body. I use this solution to examine flow through a dipping overpressured sand body (after Flemings 2002). I assume the pressure gradient far from the sandstone is equal to the lithostatic gradient, which satisfies Philips' far-field boundary conditions for constant rock and fluid properties. The vertical fluid velocity is:

$$V_z = \frac{-k}{\mu}\frac{dP^*}{dz}. \qquad \textbf{C2}$$

I Calculate V_z for typical basinal conditions assuming the following characteristics (Stump & Flemings, 2002):

$k = 1.15\times10^{-19} m^2$
$\mu = 1\times10^{-3} kg/ms$
$dP^* = 27.97 MPa$
$dZ = 4414 m$

V_z is therefore,

$$V_z = \frac{-1.15\times10^{-19}}{1\times10^{-3}}\frac{27.97\times10^{6}}{4414}, \qquad \textbf{C3}$$

$$V_z = 7.2871\times10^{-13} ms^{-1},$$

or

$$V_z = 0.02298 mm/yr .$$

A sandstone body with maximum length (l) will drain an area of $2l$ and thus the fluid flux (q) for Auger will be:

$$q = V_z 2l$$
$$q = 0.02298 mmyr^{-1}\times 2\left(36.95km\right)$$
$$q = 5.377\times10^{-8} m^2 s^{-1}$$

If this flux was to occur through the Q sand the change in pressure gradient would be:

$$\frac{dP^*}{dZ} = \frac{q\mu}{kh}. \qquad \textbf{C4}$$

I assume that the sand permeability is (k) 400md ($3.94\text{x}10^{-13}\text{m}^2/\text{s}$) and the height (h) is 30m.

The gradient generated by this flow though the Q sand would be:

$$\frac{dP^*}{dZ} = \frac{(5.4\times10^{-8})\times(1\times10^{-3})}{(3.94\times10^{-13})\times30} \qquad \textbf{C5}$$
$$\frac{dP^*}{dZ} = 4.54 Pa/m$$

This change in gradient is very small. Therefore, even though flow is occurring, there is almost no measurable change from the hydrostatic gradient. Thus when I extrapolate sand pressures to their structural limits I assume a hydrostatic gradient.

References

ABRAMS, M.A., BOETTCHER, S.S. & ANONYMOUS (2000) Mapping Migration Pathways Using Geophysical Data, Seabed Core Geochemistry and Submersible Observations in the Central Gulf of Mexico. *American Association of Petroleum Geologists 2000 annual meeting*, American Association of Petroleum Geologists and Society of Economic Paleontologists and Mineralogists (AAPG). Tulsa, OK. **2000,** 1.

ABRAMS, M.A. (2005) Significance of Hydrocarbon Seepage Relative to Petroleum Generation and Entrapment. *Near-surface hydrocarbon migration; mechanisms and seepage rates*. M. A. Abrams & J. K. Whelan, Elsevier. Oxford. **22,** 457-477.

ABRAMS, M.A. & WHELAN, J.K. (2005) Near-Surface Hydrocarbon Migration Mechanisms and Seepage Rates. *Near-surface hydrocarbon migration; mechanisms and seepage rates*. M. A. Abrams & J. K. Whelan, Elsevier. Oxford. **22**.

AHARON, P. (2003) Is Drilling in Deepwater Gulf of Mexico Uncorking Bad Genies? *Transactions of the 53rd annual convention; 50th GCSSEPM anniversary*. G. W. Stone, J. H. Wrenn & S. J. Bentley, Gulf Coast Association of Geological Societies. New Orleans, LA. **53,** 1-10.

ATHY, L.F. (1930) Density, Porosity, and Compaction of Sedimentary Rocks. *AAPG Bulletin*. **14,** 1-24.

BIRCHWOOD, K.M. (1965) Mud Volcanoes in Trinidad. *Insitute of Petroleum Reviews*. **19,** 164-167.

BOHN, C.W., REILLY, M.J., SEREN, D.X., VALENTI, J.C.A.F., FLEMINGS, P.B. & ERTEKIN, T. (2008) Characterization of the N and O Sands of the Auger Basin, Gulf of Mexico. *M.S. Joint Thesis, Submitted for publication*.

BOOTH, J.R., DUVERNAY, A.E., PFEIFFER, D.S. & STYZEN, M.J. (2000) Sequence Stratigraphic Framework, Depositional Models, and Stacking Patterns of Ponded and Slope Fan Systems in the Auger Basin: Central Gulf of Mexico. *GCSEPM Foundation 20th Annual Research Conference, Deep-Water Reservoirs of the World*.

BOOTH, J.R., DEAN, M.C., DUVERNAY, A.E. & STYZEN, M.J. (2003) Paleo-Bathymetric Controls on the Stratigraphic Architecture and Reservoir Development of Confined Fans in the Auger Basin; Central Gulf of Mexico Slope. *Turbidites; models and problems*. G. S. Steffens, C. Pirmez, M. Orlando & D. Roberts, Elsevier. Oxford. **20,** 563-586.

DAVIES, R.J. & STEWART, S.A. (2005) Emplacement of Giant Mud Volcanoes in the South Caspian Basin: 3d Seismic Reflection Imaging of Their Root Zones. *Journal of the Geological Society, London*. **162,** 1-4.

DAVIES, R.J., SWARBRICK, R.E., EVANS, R.J. & HUUSE, M. (2007) Birth of a Mud Volcano; East Java, 29 May 2006. *GSA Today*, Geological Society of America (GSA). Boulder, CO. **17,** 4-9.

DAVIES, R.J., BRUMM, M., MANGA, M., RUBIANDINI, R., SWARBRICK, R. & TINGAY, M. (2008) The East Java Mud Volcano (2006 to Present): An Earthquake or Drilling Trigger? *Earth and Planetary Science Letters*, **In Press**.

FLEMINGS, P.B., STUMP, B.B., FINKBEINER, T. & ZOBACK, M. (2002) Flow Focusing in Overpressured Sandstones; Theory, Observations, and Applications. *American Journal of Science*, Yale University, Kline Geology Laboratory. New Haven, CT. **302,** 827-855.

GAARENSTROOM, L., TROMP, R.A.J., DE JONG, M.C. & BRANDENBURG, A.M. (1993) Overpressures in the Central North Sea; Implications for Trap Integrity and Drilling Safety. *Petroleum geology of Northwest Europe; Proceedings of the 4th conference*. J. R. Parker, The=Geological Society of London. London. **4,** 1305-1313.

GRAUE, K. (2000) Mud Volcanoes in Deepwater Nigeria. *Marine and Petroleum Geology*, Elsevier. Oxford. **17,** 959-974.

HARRISON, W.J. & SUMMA, L.L. (1991) Paleohydrology of the Gulf of Mexico Basin. *American Journal of Science*, Kline Geology Laboratory, Yale University. New Haven, CT. **291,** 109-176.

HEDBERG, H.D. (1974) Relation of Methane Generation to Undercompacted Shales, Shale Diapirs, and Mud Volcanoes. *AAPG Bulletin*. **58,** 661-673.

HIGGINS, G.E. & SAUNDERS, J.B. (1974) Mud Volcanoes; Their Nature and Origin. *Contributions to the Geology and Paleobiology of the Caribbean and Adjacent Areas*, Birkhaeuser Verlag. Basel. **84,** 101-152.

HOOD, K.C., WENGER, L.M., GROSS, O.P. & HARRISON, S.C. (2002) Hydrocarbon Systems Analysis of the Northern Gulf of Mexico; Delineation of Hydrocarbon Migration Pathways Using Seeps and Seismic Imaging. *Surface exploration case histories; applications of geochemistry, magnetic, and remote sensing*. D. Schumacher & L. A. LeSchack, American Association of Petroleum Geologists. Tulsa, OK. **48,** 25-40.

KENDRICK, J.W. (1999) Turbidite Reservoir Architecture in the Gulf of Mexico; Insights from Field Development. *AAPG international conference and exhibition; abstracts*, American Association of Petroleum Geologists. Tulsa, OK. **83,** 1322.

KHALILOV, N.Y. & KERIMOV, A.A. (1983) Origin of Mud Volcanism and Diapirism, Winston & Son. Silver Spring, MD. **25,** 877-881.

KOHL, B. & ROBERTS, H.H. (1994) Fossil Foraminifera from Four Active Mud Volcanoes in the Gulf of Mexico. *Hydrocarbon seeps and vents*. P. Aharon, Springer International. Berlin-Heidelberg. **14,** 126-134.

LUPA, J., FLEMINGS, P. & TENNANT, S. (2002) Pressure and Trap Integrity in the Deepwater Gulf of Mexico. *The Leading Edge*. **21,** 184-187.

MACDONALD, I.R., BUTHMAN, D.B., SAGER, W.W., PECCINI, M.B. & GUINASSO, N.L., JR. (2000) Pulsed Oil Discharge from a Mud Volcano. *Geology*. **28,** 907-910.

MACDONALD, I.R., LEIFER, I., SASSEN, R., STINE, P., MITCHELL, R. & GUINASSO, N. (2002) Transfer of Hydrocarbons from Natural Seeps to the Water Column and Atmosphere. *Geofluids*, Blackwell Science. Oxford. **2,** 95-107.

MAZZINI, A., SVENSEN, H., AKHMANOV, G.G., ALOISI, G., PLANKE, S., MALTHE-SORENSSEN, A. & ISTADI, B. (2007) Triggering and Dynamic Evolution of the Lusi Mud Volcano, Indonesia. *Earth and Planetary Science Letters*, Elsevier. Amsterdam. **261,** 375-388.

MCGEE, D.T., BILINSKI, P.W., GARY, P.S., PFEIFFER, D.S., SHEIMAN, J.L. & ANONYMOUS (1993) Geologic Models and Reservoir Geometries of Auger Field, Deepwater Gulf of Mexico. *American Association of Petroleum Geologists 1993 annual convention*, American Association of Petroleum Geologists and Society of Economic Paleontologists and Mineralogists. Tulsa, OK. **1993,** 149.

ROBERTS, H.H. & CARNEY, R.S. (1997) Evidence of Episodic Fluid, Gas, and Sediment Venting on the Northern Gulf of Mexico Continental Slope. *Economic Geology*. **92,** 863-879.

ROEGIERS, J.-C. (1989) Elements of Rock Mechanics, . *in Economides, M.J., and Nolte, K.G., editors, Reservoir simulation: Englewood Cliffs, New Jersey, Prentice Hall***,** 2-1, 2-22.

SELDON, B. & FLEMINGS, P.B. (2005) Reservoir Pressure and Seafloor Venting: Predicting Trap Integrity in a Gulf of Mexico Deepwater Turbidite Minibasin. *AAPG Bulletin*. **89,** 193-209.

SHEW, R.D., GARY, P.S., PFEIFFER, D.S., BILINSKI, P.W. & ANONYMOUS (1993) Evidence and Importance of a Pliocene, Carbonate-Rich Deposit Formed in Association with a Hydrocarbon Seep at Auger Field. *American Association of Petroleum Geologists 1993 annual convention*, American Association of Petroleum Geologists and Society of Economic Paleontologists and Mineralogists. Tulsa, OK. **1993,** 181.

STEWART, S.A. & DAVIES, R.J. (2006) Structure and Emplacement of Mud Volcano Systems in the South Caspian Basin. *AAPG Bulletin*. **90,** 771-786.

STUMP, B.B. & FLEMINGS, P.B. (2002) Consolidation State, Permeability, and Stress Ratio as Determined from Uniaxial Strain Experiments on Mudstone Samples from the Eugene Island 330 Area, Offshore Louisiana. *Pressure regimes in sedimentary basins and their prediction*. A. R. Huffman & G. L. Bowers, American Association of Petroleum Geologists. Tulsa, OK. **76,** 131-144.

SWARBRICK, R.E., OSBORNE, M.J., GRUNBERGER, D., YARDLEY, G.S., MACLEOD, G., APLIN, A.C., LARTER, S.R., KNIGHT, I. & AULD, H.A. (2000) Integrated Study of the Judy Field (Block 30/7a); an Overpressured Central North Sea Oil/Gas Field. *Marine and Petroleum Geology*, Elsevier. Oxford. **17,** 993-1010.

TINGAY, M., HEIDBACH, O., DAVIES, R.J. & SWARBRICK, R.E. (2008) Triggering of the Lusi Mud Eruption: Earthquake Versus Drilling Initation. *Geology*, **36,** 639-642.

TURCOTTE, D.L. & SCHUBERT, G. (1982) Geodynamics: Aplications of Continuum Physics to Geological Problems. *450pp., John Wiley and Sons, New York.*

YASSIR, N.A. (1987) Mud Volcanoes; Evidence of Neotectonic Activity. *Papers presented at the first Sino-British geological conference on geotechnical engineering and hazard assessment in neotectonic terrains*. J.-J. Hung & L. S. Teng, Chung Kuo Ti Chih Hseuh Hui. Taipei. **9,** 513-524.